



- 1 Sources and characteristics of size-resolved particulate organic acids and methanesulfonate in a  
2 coastal megacity: Manila, Philippines
- 3 Connor Stahl<sup>1</sup>, Melliza Templonuevo Cruz<sup>2,3</sup>, Paola Angela Bañaga<sup>2,4</sup>, Grace Betito<sup>2,4</sup>, Rachel A.  
4 Braun<sup>1</sup>, Mojtaba Azadi Aghdam<sup>1</sup>, Maria Obiminda Cambaliza<sup>2,4</sup>, Genevieve Rose Lorenzo<sup>2,5</sup>,  
5 Alexander B. MacDonald<sup>1</sup>, Miguel Ricardo A. Hilario<sup>2</sup>, Preciosa Corazon Pabroa<sup>6</sup>, John Robin  
6 Yee<sup>6</sup>, James Bernard Simpas<sup>2,4</sup>, Armin Sorooshian<sup>1,5</sup>
- 7 <sup>1</sup>Department of Chemical and Environmental Engineering, University of Arizona, Tucson,  
8 Arizona, 85721, USA
- 9 <sup>2</sup>Manila Observatory, Quezon City, 1108, Philippines
- 10 <sup>3</sup>Institute of Environmental Science and Meteorology, University of the Philippines, Diliman,  
11 Quezon City, 1101, Philippines
- 12 <sup>4</sup>Department of Physics, School of Science and Engineering, Ateneo de Manila University,  
13 Quezon City, 1108, Philippines
- 14 <sup>5</sup>Department of Hydrology and Atmospheric Sciences, University of Arizona, Tucson, Arizona,  
15 85721, USA
- 16 <sup>6</sup> Philippine Nuclear Research Institute - Department of Science and Technology,  
17 Commonwealth Avenue, Diliman, Quezon City, 1101, Philippines
- 18 *Correspondence to: armin@email.arizona.edu*



## 19 Abstract

20 A 16-month (July 2018 – October 2019) dataset of size-resolved aerosol composition is used to  
21 examine the sources and characteristics of five organic acids (oxalate, succinate, adipate,  
22 maleate, phthalate) and methanesulfonate (MSA) in Metro Manila, Philippines. As one of the  
23 most polluted megacities globally, Metro Manila offers a view of how diverse sources and  
24 meteorology impact the relative amounts and size distributions of these species. A total of 66  
25 sample sets were collected with a Micro-Orifice Uniform Deposit Impactor (MOUDI), of which  
26 54 sets were analyzed for composition. Organic acids and MSA surprisingly were less abundant  
27 than in other global regions that are also densely populated. The combined species accounted for  
28 an average of  $0.80 \pm 0.66$  % of total gravimetric mass between 0.056 and 18  $\mu\text{m}$ , leaving still  
29 33.74 % of mass unaccounted for after considering black carbon and water-soluble ions and  
30 elements. The unresolved mass is suggested to consist of non-water-soluble metals as well as  
31 both water-soluble and non-water-soluble organics. Oxalate was approximately an order of  
32 magnitude more abundant than the other five species ( $148.59 \pm 94.26$   $\text{ng m}^{-3}$  versus others being  
33  $< 10$   $\text{ng m}^{-3}$ ). Both PMF and correlation analysis is conducted with tracer species to investigate  
34 the possible sources for organic acids and MSA. Enhanced biomass burning influence in the  
35 2018 southwest monsoon (SWM18) resulted in especially high levels of submicrometer  
36 succinate, MSA, oxalate, and phthalate. Peculiarly, MSA had negligible contributions from  
37 marine sources but instead was linked to burning and combustion. Enhanced precipitation during  
38 the two SWM seasons (8 June – 4 October 2018 and 14 June – 7 October 2019) coincided with  
39 stronger influence from local emissions rather than long-range transport, leading to notable  
40 concentration enhancements in both the sub- and supermicrometer ranges for some species (e.g.,  
41 maleate and phthalate). While secondary formation via gas-to-particle conversion largely  
42 explained submicrometer peaks for all species, several species (i.e., phthalate, adipate, succinate,  
43 oxalate) exhibited a prominent peak in the coarse mode, largely owing to their association with  
44 crustal emissions (i.e., more alkaline aerosol type) rather than sea salt. Oxalate's strong  
45 association with sulfate in the submicrometer mode supports an aqueous-phase formation  
46 pathway for the study region, but also high concentration during periods of low rain and high  
47 solar radiation indicates photo-oxidation is an important formation pathway.



## 48 1. Introduction

49 Organic acids are ubiquitous components of ambient particulate matter and can contribute  
50 appreciably to total mass concentrations in diverse regions ranging from the Arctic to deserts  
51 (e.g. Barbaro et al., 2017; Ding et al., 2013; Duarte et al., 2017; Gao et al., 2003; Kondo et al.,  
52 2011; Skyllakou et al., 2017; Sun et al., 2012; Youn et al., 2013). Furthermore, another class of  
53 species contributing to ambient aerosol mass is organosulfur compounds, with methanesulfonate  
54 (MSA) being an example species (Bardouki et al., 2003b; Ding et al., 2017; Falkovich et al.,  
55 2005; Kerminen et al., 1999; Maudlin et al., 2015; Ziemba et al., 2011). The spatiotemporal and  
56 size-resolved mass concentration profiles of organic and sulfonic acids are difficult to  
57 characterize and can significantly vary depending on the time of day, season, region, and  
58 meteorological profile (Adam et al., 2020; Bagtasa et al., 2019; Kobayashi et al., 2004; Maudlin  
59 et al., 2015; Mochida et al., 2003; Reid et al., 2013). It is necessary to quantify their relative  
60 abundances, and to understand factors affecting their production and eventual removal to be able  
61 to quantify their influence on aerosol hygroscopic and optical properties (Beaver et al., 2008; Cai  
62 et al., 2017; Freedman et al., 2009; Marsh et al., 2017; Marsh et al., 2019; Myhre and Nielsen,  
63 2004; Peng et al., 2016; Xue et al., 2009). Low molecular weight organic acids are water-soluble  
64 and can range widely in hygroscopicity when in their pure salt form depending on factors such as  
65 carbon number (Prenni et al., 2001; Saxena and Hildemann, 1996; Sorooshian et al., 2008) and  
66 interactions with other components in multi-component aerosol particles (Drozd et al., 2014).  
67 Organic acids are generally believed to effectively scatter light and have a cooling effect on  
68 climate (McGinty et al., 2009; Myhre and Nielsen, 2004), although their overall impact on  
69 properties such as refractive index in multicomponent aerosols is poorly characterized.  
70 Refractive indices for species investigated in this work range widely from 1.43 (MSA) to 1.62  
71 (phthalic acid). MSA is assumed to be purely scattering similar to sulfate (Hodshire et al., 2019)  
72 and to have hygroscopic properties close to those of ammonium sulfate (Asmi et al., 2010;  
73 Fossum et al., 2018). However, its hygroscopic and optical behavior is not fully understood, and  
74 is still an active area of research (Liu et al., 2011; Peng and Chan, 2001; Tang et al., 2019; Tang  
75 et al., 2015; Zeng et al., 2014).

76 Decades of research into atmospheric organic acids and MSA have yielded rich insights into  
77 their sources, production mechanisms, and fate in the atmosphere (Baboukas et al., 2000;  
78 Bardouki et al., 2003a; Gondwe et al., 2004; Kawamura and Bikkina, 2016; Limbeck et al.,  
79 2001; Norton et al., 1983; Ovadnevaite et al., 2014; Sorooshian et al., 2009; van Pinxteren et al.,  
80 2015). MSA is produced predominantly from the oxidation of dimethylsulfide (DMS) emitted  
81 from oceans (Bates et al., 2004; Davis et al., 1998; Kerminen et al., 2017), but it also can be  
82 linked to biomass burning, urban, and agricultural emissions (Sorooshian et al., 2015). Sources  
83 of organic acids include primary emissions from biomass burning, biogenic activity, and the  
84 combustion of fossil fuels (Kawamura and Kaplan, 1987) and secondary formation via gas-to-  
85 particle conversion processes stemming from both biogenic (Carlton et al., 2006) and  
86 anthropogenic emissions (Sorooshian et al., 2007b). Secondary processing can include both  
87 aqueous phase chemistry in clouds (Blando and Turpin, 2000; Ervens, 2018; Ervens et al., 2014;  
88 Hoffmann et al., 2019; Rose et al., 2018; Sareen et al., 2016; Warneck, 2005) and photo-  
89 oxidation of volatile organic compounds (VOCs) in cloud-free air (Andreae and Crutzen, 1997;



90 Gelencsér and Varga, 2005). These various sources and production pathways result in mono- and  
91 dicarboxylic acids being prevalent across a range of aerosol sizes (Bardouki et al., 2003b;  
92 Kavouras and Stephanou, 2002; Neusüss et al., 2000; Yao et al., 2002). Little is reported in terms  
93 of the size-resolved nature of organic acids and MSA over long periods of time with high  
94 sampling frequency. Although insights have already been gathered from size-resolved  
95 measurement studies (Table S1), most measurement reports are based on bulk mass  
96 concentration measurements (Chebbi and Carlier, 1996; Kawamura and Bikkina, 2016).  
97 Studying the seasonal variations of size-resolved organic acid and MSA aerosols could prove  
98 vital in improved understanding of their formation and removal mechanisms, and associated  
99 sensitivity to seasonally dependent sources and meteorological factors.

100 The Philippines is an important region to study aerosols due to the wide range in both  
101 meteorological conditions and diverse local and regional emissions sources (Alas et al., 2018;  
102 Bagtasa and Yuan, 2020; Braun et al., 2020; Hilario et al., 2020a; Kecorius et al., 2017). In  
103 addition to aerosol sources from nearby regions (Hilario et al., 2020b), the Philippines also has a  
104 significant source of local pollution largely consisting of vehicular emissions due to high  
105 population density (Madueño et al., 2019), the use of outdated vehicles (Biona et al., 2017), ship  
106 exhaust from high density shipping lanes (Streets et al., 1997; Streets et al., 2000), and more  
107 lenient air regulations leading to significant air pollution due to rapid growth and urbanization  
108 (Alas et al., 2018; Kecorius et al., 2017). This leads to Metro Manila containing some of the  
109 highest black carbon (BC) concentrations in Southeast Asia, and quite possibly the world (Alas  
110 et al., 2018; Hopke et al., 2011; Kecorius et al., 2017; Kim Oanh et al., 2006). Past aerosol  
111 characterization work for that region has focused mainly on gravimetric analysis for total bulk  
112 mass (e.g., PM<sub>2.5</sub>, PM<sub>10</sub>) (Bagtasa et al., 2018; Bagtasa et al., 2019; Cohen et al., 2009; Kim  
113 Oanh et al., 2006), water-soluble inorganic and organic ion speciation (AzadiAghdam et al.,  
114 2019; Braun et al., 2020; Cruz et al., 2019; Kim Oanh et al., 2006; Simpás et al., 2014; Stahl et  
115 al., 2020b), and BC analysis (Alas et al., 2018; Bautista et al., 2014; Kecorius et al., 2017;  
116 Takahashi et al., 2014). In an analysis of two size-resolved aerosol sets in Manila, a significant  
117 portion of the total mass unaccounted for by the water-soluble inorganic, water-soluble organic,  
118 and BC components was attributed to (but not limited to) organics and non-water soluble metals  
119 (Cruz et al., 2019). However, a concentrated effort to characterize the contributions of the water-  
120 soluble organic acids to the total aerosol mass in Manila over the course of a full year has not  
121 been undertaken.

122 The aim of this study is to use a 16 month-long dataset of size-resolved composition in Quezon  
123 City in Metro Manila to address the following questions: (i) how much do organic acids and  
124 MSA contribute to the region's aerosol mass concentrations?; (ii) what are the seasonal  
125 differences in the mass size distribution profile of organic acids and MSA, and what drives the  
126 changes?; and (iii) what are the sources and predominant formation mechanisms of these species  
127 in the sub- and super-micrometer diameter ranges? The results of this study are put in broad  
128 context by comparing findings to those in other regions.

129

## 130 **2. Methods**



## 131 2.1 Study site description

132 Metro Manila is comprised of 16 cities and a municipality totaling to a population of about 12.88  
133 million people and a collective population density of 20,800 km<sup>-2</sup> (Alas et al., 2018; PSA, 2016).  
134 Quezon City is the most populated city in Metro Manila containing 2.94 million people with a  
135 population density of 18,000 km<sup>-2</sup> (PSA, 2016), which is amidst the highest in the world.  
136 Because of these reasons, Metro Manila is a quintessential location for examining locally  
137 produced anthropogenic aerosols superimposed on a variety of other marine and continentally  
138 influenced air masses transported from upwind regions (Kim Oanh et al., 2006).

139 Measurements were conducted over a 16-month period between July 2018 and October 2019 at  
140 Manila Observatory (MO; 14.64° N, 121.08° E) on the third floor (~85 m a.s.l.) of an office  
141 building, which is on the Ateneo de Manila University campus in Quezon City, Philippines (Fig.  
142 1). Sampling was conducted approximately 100 m away from the nearest road on campus and  
143 therefore campus emissions do not impact sampling to a large degree, qualifying the monitoring  
144 site as an urban mixed background site (Hilario et al., 2020a) capturing local, regional, and long-  
145 range transported emissions. The following four seasons were the focus of the sampling period:  
146 the 2018 southwest monsoon (SWM18, 8 June – 4 October 2018) (PAGASA, 2018a, c), a  
147 transitional period (Trans, 5 – 25 October 2018), the northeast monsoon (NEM, 26 October 2018  
148 – 13 June 2019) (PAGASA, 2018b), and the 2019 southwest monsoon (SWM19, 14 June – 7  
149 October 2019) (PAGASA, 2019b, a). These seasons have also been defined in other works (i.e.,  
150 Akasaka et al., 2007; Cruz et al., 2013; Matsumoto et al., 2020) and can predominately be  
151 separated into two general seasons, wet (SWM) and dry (NEM). Generally, there is a second  
152 transitional period in May that transitions between the NEM and SWM (Bagtasa and Yuan,  
153 2020), however, recent studies suggest that the transition is abrupt (Matsumoto et al., 2020).  
154 Consequently, the second transitional period was combined with the NEM season.

## 155 2.2 Instrument description

156 Ambient aerosol was collected with a Micro-Orifice Uniform Deposit Impactor II (MOUDI II  
157 120R, MSP Corporation, Marple et al. (2014)) using Teflon substrates (PTFE membrane, 2 μm  
158 pores, 46.2 mm diameter, Whatman). The MOUDI-II is a 10-stage impactor with aerodynamic  
159 cutpoint diameters ( $D_p$ ) of 10, 5.6, 3.2, 1.8, 1.0, 0.56, 0.32, 0.18, 0.10, and 0.056 μm with a  
160 nominal flow rate of ~30 L min<sup>-1</sup>. A total of 66 MOUDI sets were collected on a weekly basis  
161 usually over a 48-hour period; however, only 54 sets were analyzed for ions and 47 of those  
162 sets were also analyzed for elements. A 48-hour period was chosen because it offered an optimal  
163 compromise between gathering samples with fine temporal resolution and samples with a  
164 sufficiently large chemical signal to exceed analytical limits of detection. Details of the sample  
165 sets are shown in Table S2 can be found in more detail in Stahl et al. (2020b).

166 Water-soluble organic acids, MSA, and inorganic ions were speciated and quantified using ion  
167 chromatography (IC; Thermo Scientific Dionex ICS-2100 system) with a flowrate of 0.4 mL  
168 min<sup>-1</sup>. The anionic species of relevance to this study were MSA, chloride (Cl<sup>-</sup>), nitrate (NO<sub>3</sub><sup>-</sup>),  
169 sulfate (SO<sub>4</sub><sup>2-</sup>), adipate, succinate, maleate, oxalate, and phthalate. These anions were resolved  
170 using potassium hydroxide (KOH) eluent, an AS11-HC 250 mm column, and an AERS 500e



171 suppressor. The cationic species of relevance to this study was sodium ( $\text{Na}^+$ ), which was detected  
172 using methanesulfonic acid eluent, a CS12A 250 mm column, and a CERS 500e suppressor. The  
173 IC instrument methods for anion and cation analysis can be found in Stahl et al. (2020b). Water-  
174 soluble elements were measured using a triple quadrupole inductively coupled plasma mass  
175 spectrometry (ICP-QQQ; Agilent 8800 Series). The quantified elements of relevance to this  
176 study include Al, As, Cd, K, Ni, Pb, Rb, Ti, and V. Limits of detection (LOD) and recoveries  
177 were calculated for all ionic and elemental species and provided in Table S3. Aside from the  
178 species that are the focus of this study (organic acids and MSA), the other elements and ions  
179 were included as they are useful tracers for different aerosol sources to aid in source  
180 apportionment. Although pyruvate was speciated with IC, it is not considered with the other  
181 organic acids because it was below the LOD for 48 of the 54 sets. It should also be noted that  
182 only a subset of species were listed here, which were used for analyses. The full suite of species  
183 can be seen in Stahl et al. (2020b).

184 Eleven of the 66 MOUDI sets included simultaneously operated MOUDIs next to each other to  
185 complement the chemical speciation analysis with gravimetric analysis. A Sartorius ME5-F  
186 microbalance (sensitivity of  $\pm 1 \mu\text{g}$ ) was used in an air-buffered room with controlled  
187 temperature ( $20 - 23 \text{ }^\circ\text{C}$ ) and relative humidity (RH:  $30 - 40 \%$ ). Each substrate was passed near  
188 an antistatic tip for approximately 30 seconds to minimize bias due to electrostatic charge.  
189 Multiple weight measurements were conducted before and after sampling, with the difference  
190 between weighings being less than  $10 \mu\text{g}$  for each condition, respectively. The difference  
191 between substrate weights before and after sampling was equated to total gravimetric mass.

192 Black carbon was measured using a Multi-wavelength Absorption Black Carbon Instrument  
193 (MABI; Australian Nuclear Science and Technology Organisation). The MABI optically  
194 quantifies black carbon concentrations by detecting the absorption at seven wavelengths (405,  
195 465, 525, 639, 870, 940, and 1050 nm); however, the wavelength at 870 nm is used here as black  
196 carbon is the primary absorber at that wavelength (Cruz et al., 2019; Ramachandran and Rajesh,  
197 2007; Ran et al., 2016).

198 Meteorological parameters were measured at MO during the study period using a Davis Vantage  
199 Pro2<sup>TM</sup> Plus automatic weather station, which was located on the roof of MO. Measured  
200 parameters of relevance included temperature, accumulated rain, RH, and solar radiation. Data  
201 were collected in five-minute increments and were cleaned based on the method of Bañares et al.  
202 (2018) to verify values were in acceptable ranges. The meteorological parameters, except for  
203 rain, were averaged over each sampling period while rain was summed over time to obtain the  
204 accumulated precipitation for a sampling period. There were two periods where the automatic  
205 weather station located at MO had missing values, 6 November – 27 November 2018 and 7  
206 August – 3 September 2019. In these cases, missing values were substituted with values from a  
207 secondary automatic weather station located approximately 2 km away ( $14.63^\circ \text{N}$ ,  $121.06^\circ \text{E}$ ),  
208 and if missing data still persisted, a tertiary station located 5 km away ( $14.67^\circ \text{N}$ ,  $121.11^\circ \text{E}$ ) was  
209 used. Identical data cleaning procedures were implemented for the secondary and tertiary sites.

210



### 211 2.3 Concentration weighted trajectories (CWT)

212 A CWT analysis was conducted to identify sources of detected species. The method assigns a  
213 weighted concentration to a grid that is calculated by finding the mean of sample concentrations  
214 that have trajectories crossing a particular cell in the grid (e.g., Dimitriou, 2015; Dimitriou et al.,  
215 2015; Hilario et al., 2020a; Hsu et al., 2003). The software TrajStat (Wang et al., 2009)  
216 determines CWT profiles by using back-trajectories from the NOAA Hybrid Single-Particle  
217 Lagrangian Integrated Trajectory (HYSPPLIT) model (Rolph et al., 2017; Stein et al., 2015).  
218 Three-day back-trajectories were obtained with an ending altitude of 500 m above ground level  
219 using the Global Data Assimilation System (GDAS) and the “Model vertical velocity” method.  
220 The choice of 500 m is based on representativeness of the mixed layer and having been widely  
221 used in other studies (e.g., Crosbie et al., 2014; Mora et al., 2017; Sorooshian et al., 2011).  
222 Trajectories were obtained every 6 hours after MOUDI sampling began for each sample set,  
223 yielding approximately nine trajectories per set. A grid domain of 95° to 150° E longitude and -  
224 5° to 45° N latitude was used with a grid cell resolution of 0.5° × 0.5°. The analysis was  
225 performed for each measured organic acid and MSA for the full diameter range of MOUDI sets  
226 (0.056 – 18 μm). A weighting function was applied to the CWT plots to minimize uncertainty;  
227 hereafter CWT plots will be referred as WCWT plots.

228

### 229 2.4 Positive matrix factorization (PMF)

230 PMF analysis was applied to identify sources and their relative importance for the mass  
231 concentration budgets of the species discussed in this work. Model simulations were conducted  
232 based on MOUDI data for the diameter range of 0.056 – 18 μm. Nineteen species (Al, Ti, K, Rb,  
233 V, Ni, As, Cd, Pb, Na<sup>+</sup>, Cl<sup>-</sup>, NO<sub>3</sub><sup>-</sup>, SO<sub>4</sub><sup>2-</sup>, MSA, adipate, succinate, maleate, oxalate, and  
234 phthalate) were included in the analysis and categorized as “strong”. Each individual stage of  
235 MOUDI sets was considered an independent variable for the analysis. Missing values or values  
236 below detection limit were replaced with zeros with the exception of sets where ICP-QQQ  
237 analysis was not performed (57, 59, 60, 61, 62, 64, 65). Those missing values were replaced with  
238 the geometric mean for each respective stage. The uncertainty for each stage and species was  
239 calculated as follows:

$$240 \text{ Uncertainty} = 0.05 * [x] + LOD \quad (\text{Eq. 1})$$

241 where [x] is the concentration of the species (Reff et al., 2007). No additional uncertainty was  
242 added to account for any unconsidered errors for all species. The uncertainty of the model output  
243 was evaluated using displacement (DISP), bootstrapping (BS), and bootstrapping with  
244 displacement (BS-DISP). For BS, 100 resamples were used and a value of 0.6 was used as a  
245 threshold for the correlation coefficient (r) to pass as successful mapping for each simulation.

246 To qualify as a valid result, reported PMF results had to meet the following criteria: (i) factors  
247 mapped with BS runs, (ii) no factor swaps in DISP, (iii) dQ values being close or equal to 0%,  
248 and (iv) no factor swaps in BS-DISP where Al, Ti, K, Rb, V, Ni, As, Cd, Pb, Na<sup>+</sup>, Cl<sup>-</sup>, NO<sub>3</sub><sup>-</sup>, and



249  $\text{SO}_4^{2-}$  were displaced. PMF diagnostics can be seen in Table S4 based on the method of Brown et  
250 al. (2015).

251

### 252 3. Results

253 A brief overview of the species being examined is first provided before reviewing concentration  
254 statistics. MSA is an oxidation product of dimethylsulfide (DMS) emitted primarily from the  
255 ocean (Berresheim, 1987; Saltzman et al., 1983), but it can also be formed from dimethyl  
256 sulphoxide (DMSO) emitted from anthropogenic sources such as industrial waste (Yuan et al.,  
257 2004). Gaseous MSA can become associated with particulate matter via new particle formation  
258 (Dawson et al., 2012), and through heterogeneous reactions or condensation onto existing  
259 particles (De Bruyn et al., 1994; Hanson, 2005). Of the three saturated dicarboxylic acids,  
260 succinate ( $\text{C}_4$ ) and adipate ( $\text{C}_6$ ) are larger chain dicarboxylic acids linked to ozonolysis of cyclic  
261 alkenes, which is common in areas with extensive vehicular emissions (Grosjean et al., 1978;  
262 Hatakeyama et al., 1987). They can also be emitted via processes such as meat cooking (Rogge  
263 et al., 1993) and biomass burning (Kawamura et al., 2013; Pereira et al., 1982) and can be  
264 secondarily formed by the photo-oxidation of higher chain organic acids, such as azelaic acid  
265 (Bikkina et al., 2014; Ervens et al., 2004). Oxalate ( $\text{C}_2$ ) is the smallest of those three acids and is  
266 usually the most abundant on a mass basis of all dicarboxylic acids in tropospheric aerosols as it  
267 represents an end-product in the oxidation of both larger-chain carboxylic acids and also  
268 glyoxylic acid (Ervens et al., 2004). It can be emitted via direct emissions such as from biomass  
269 burning (Graham et al., 2002; Narukawa et al., 1999; Xu et al., 2020), combustion exhaust  
270 (Kawamura and Kaplan, 1987; Kawamura and Yasui, 2005; Wang et al., 2010), and from  
271 various biogenic sources (Kawamura and Kaplan, 1987). Maleate ( $\text{C}_4$ ) is an unsaturated  
272 dicarboxylic acid originating from combustion engines, including via direct emissions  
273 (Kawamura and Kaplan, 1987) and secondarily produced from the photo-oxidation of benzene  
274 (Rogge et al., 1993). Lastly, phthalate ( $\text{C}_8$ ) represents an aromatic dicarboxylic acid associated  
275 with incomplete combustion of vehicular emissions (Kawamura and Kaplan, 1987) and oxidation  
276 of naphthalene or other polycyclic aromatic hydrocarbons (Fine et al., 2004; Kawamura and  
277 Ikushima, 2002; Kawamura and Yasui, 2005). However, it has also been linked to biomass  
278 burning (Kumar et al., 2015) and burning of plastic material such as polyvinyl chloride (PVC)  
279 products, garbage, and plastic bags (Agarwal et al., 2020; Claeys et al., 2012; Fu et al., 2012; Li  
280 et al., 2019; Nguyen et al., 2016; Simoneit et al., 2005). Secondary formation via aqueous-phase  
281 chemistry has been documented for these organic acids (Kunwar et al., 2019; Sorooshian et al.,  
282 2007a; Sorooshian et al., 2010; Sorooshian et al., 2006; Wonaschuetz et al., 2012) and MSA  
283 (Hoffmann et al., 2016).

284 Meteorological data are next summarized based on average values temporally coincident with  
285 each MOUDI sample set period for each of the seasons. The exception to this was the  
286 accumulated rainfall, which was summed for the MOUDI set duration. Temperatures were stable  
287 during the different seasons:  $28.0 \pm 1.04$  °C (SWM18),  $28.9 \pm 0.8$  °C (Trans),  $28.3 \pm 1.9$  °C  
288 (NEM), and  $28.4 \pm 1.5$  °C (SWM19). Solar radiation was the highest during the Trans ( $279.61 \pm$   
289  $19.68$   $\text{W m}^{-2}$ ) and NEM ( $304.01 \pm 67.54$   $\text{W m}^{-2}$ ) seasons, and lowest during the SWM18 ( $225.32$



290  $\pm 56.26 \text{ W m}^{-2}$ ) and SWM19 ( $256.05 \pm 86.88 \text{ W m}^{-2}$ ) seasons owing largely to more cloud cover.  
291 Accumulated rain was highest for both SWM seasons (SWM18:  $29.78 \pm 27.28 \text{ mm}$ ; SWM19:  
292  $16.66 \pm 23.98 \text{ mm}$ ) and much lower during the Trans ( $1.00 \pm 1.11 \text{ mm}$ ) and NEM ( $2.20 \pm 6.70$   
293  $\text{mm}$ ) seasons. Relative humidity was relatively consistent across seasons: SWM18 ( $69.6 \pm 5.0$   
294 %), Trans ( $69.2 \pm 2.2 \%$ ), NEM season ( $62.4 \pm 8.0 \%$ ), SWM19 ( $72.6 \pm 11.7 \%$ ). Finally, Fig. 1  
295 summarizes predominant wind patterns for each season based on HYSPLIT back-trajectories  
296 collected every 6 hours during sampling periods. The SWM18 and SWM19 seasons were  
297 characterized by predominantly southwesterly winds, while the NEM and Trans seasons  
298 experienced mostly northeasterly winds. In conclusion, there was much higher potential for wet  
299 scavenging during the SWM seasons, with the potential for more photochemical reactivity in the  
300 NEM and Trans seasons owing to enhanced incident solar radiation. As humidity was generally  
301 enhanced year-round, there was the likelihood of aqueous-phase processing to occur in all  
302 seasons. The combination of sustained RH, low boundary layer height, and high surface-level  
303 particle concentrations have been suggested to counteract the effects of wet deposition on total  
304 particle concentration in Metro Manila (Hilario et al., 2020a).

305

### 306 3.1 Bulk aerosol measurements

307 The range, mean, and standard deviation of concentrations integrated across the MOUDI  
308 diameter range ( $0.056 - 18 \mu\text{m}$ ) are shown in Table 1 for each organic acid and MSA for all  
309 seasons. In order of decreasing concentration, the following was the order of abundance based on  
310 the cumulative dataset: oxalate ( $148.59 \pm 94.26 \text{ ng m}^{-3}$ ) > succinate ( $9.53 \pm 22.25 \text{ ng m}^{-3}$ ) >  
311 maleate ( $9.52 \pm 19.66 \text{ ng m}^{-3}$ ) > phthalate ( $8.68 \pm 13.77 \text{ ng m}^{-3}$ ) > adipate ( $7.60 \pm 9.38 \text{ ng m}^{-3}$ ) >  
312 MSA ( $5.40 \pm 5.23 \text{ ng m}^{-3}$ ). The relative order of abundance varies for the sub- and super-  
313 micrometer ranges with the only consistent feature being that oxalate was the most abundant  
314 species. This result was consistent with past works showing oxalate to be the most abundant  
315 organic acid in different global regions (e.g., Decesari et al. (2006); Kerminen et al. (1999);  
316 Sorooshian et al. (2007b); Ziemba et al. (2011)).

317 Figure 2 shows the combined contribution of the organic acids and MSA to total gravimetric  
318 mass, while Table S5 summarizes percent contributions of individual species to total mass for  
319 different size bins. Combined, the measured organic acids and MSA accounted for only a small  
320 part of the total cumulative mass ( $0.80 \pm 0.66 \%$ ), ranging from  $0.23 - 1.49 \%$  across the 11  
321 individual gravimetric sets. When the combined contribution of organic acids and MSA to total  
322 gravimetric mass were separated by season, results are generally the same (Fig. S1), with  
323 differences in the percent range being as follows: SWM18 =  $0.64 \%$ ; Trans =  $0.95 \%$ ; NEM =  
324  $0.50 - 1.49 \%$ ; and SWM19 =  $0.23 - 0.83 \%$ . The highest contribution of these organic acids and  
325 MSA occurred for MOUDI sets collected 12 – 14 March 2019 during the NEM season, which  
326 accounted for  $1.49 \%$  ( $0.50 \mu\text{g m}^{-3}$ ) of the total mass. The lowest contribution of these organic  
327 acids and MSA occurred for MOUDI sets collected 11 – 13 September 2019 during the SWM19  
328 season, which accounted for  $0.23 \%$  ( $0.06 \mu\text{g m}^{-3}$ ) of the total mass. The summed contributions  
329 of the six species were nearly the same in the sub- and supermicrometer ranges ( $0.78 \pm 0.74 \%$   
330 and  $0.84 \pm 0.58 \%$ , respectively). Their contributions peaked in the two sizes bins covering the



331 range between 0.56 and 1.8  $\mu\text{m}$  (0.56 – 1  $\mu\text{m}$ :  $1.06 \pm 1.01$  %; 1 – 1.8  $\mu\text{m}$ :  $1.01 \pm 0.78$  %). After  
332 accounting for all measured species (BC, water-soluble species), there still remained  $33.74 \pm$   
333  $19.89$  % (range: 23.86 – 50.88 %) of unresolved mass. Therefore, the six species of interest in  
334 this work only explain a small amount of the region's mass concentrations and further work is  
335 still needed to resolve the remaining components, which presumably is dominated by water-  
336 insoluble organics and elements. Of most need is to resolve those missing components in the  
337 supermicrometer range, where Table S5 shows that the unresolved fraction is  $69.10 \pm 25.91$  %,   
338 in contrast to  $17.78 \pm 17.25$  % for the submicrometer range.

339 Although there are fairly wide ranges in concentration for the individual species, a few features  
340 are noteworthy based on the cumulative dataset. First, the oxalate concentrations are lower than  
341 expected for such a highly polluted area, as will be expanded upon in Sect. 4.6. Second, there is a  
342 significant decrease in concentration after oxalate for the remaining five species, which had  
343 similar mean concentrations. Lastly, although the sampling site is on an island and close to  
344 marine sources, MSA is surprisingly the least abundant among the six species of interest.

345 Mean mass concentrations of these species varied greatly by season as visually shown in Fig. 3a  
346 and summarized numerically in Table 1. In contrast, Fig. 3b shows that the mass fractions of the  
347 six species did not change much seasonally owing to the dominance of oxalate ( $37.67 - 472.82$   
348  $\text{ng m}^{-3}$ ), which accounted for between 69.1-87.3 % of the cumulative concentration of the six  
349 species across the four seasons. Important features with regard to seasonal mass concentration  
350 differences include the following: (i) maleate concentrations were much higher in the SWM18  
351 and SWM19 seasons; (ii) the lowest overall concentrations of most species, besides oxalate and  
352 succinate (lowest in SWM19), were observed in the NEM season; (iii) oxalate and phthalate  
353 were the only species that peaked in the Trans period, whereas the rest of the species peaked in  
354 either SWM18 or SWM19; and (iv) succinate and phthalate were peculiarly much more  
355 enhanced in SWM18 than SWM19, pointing to significant variability between consecutive years.

356

### 357 3.2 Source apportionment

358 To help elucidate how different emissions sources impact the six species, PMF analysis was  
359 conducted and yielded a solution with five source factors using year-round data (Fig. 4). The five  
360 sources are as follows in decreasing order of their contribution to the total mass based on the sum  
361 of species used in the PMF analysis (Fig. 4): combustion (32.1 %), biomass burning (20.9 %),  
362 sea salt (20.9 %), crustal (14.2 %), and waste processing (11.9 %). The contribution of each  
363 source to the total concentration of organic acids and MSA was as follows: combustion (33.5 %),  
364 biomass burning (29.0 %), crustal (27.0 %), waste processing (9.8 %), and sea salt (0.6 %). The  
365 source factor names were determined based on the enhancement of the following species (Fig.  
366 4): crustal (Al, Ti) (Harrison et al., 2011; Malm et al., 1994; Singh et al., 2002), biomass burning  
367 (K, Rb) (Andreae, 1983; Artaxo et al., 1994; Braun et al., 2020; Chow et al., 2004; Echalar et al.,  
368 1995; Ma et al., 2019; Schlosser et al., 2017; Thepnuan et al., 2019; Yamasoe et al., 2000), sea  
369 salt (Na, Cl) (Seinfeld and Pandis, 2016), combustion (V, Ni, As) (Allen et al., 2001; Linak et al.,  
370 2000; Mahowald et al., 2008; Mooibroek et al., 2011; Prabhakar et al., 2014; Wasson et al.,



371 2005), and waste processing (Cd, Pb) (Cruz et al., 2019; Gullett et al., 2007; Iijima et al., 2007;  
372 Pabroa et al., 2011). While both  $\text{SO}_4^{2-}$  and  $\text{NO}_3^-$  are secondarily produced, the latter is more  
373 commonly linked to supermicrometer particles (Allen et al., 1996; Dasgupta et al., 2007;  
374 Fitzgerald, 1991; Maudlin et al., 2015), including in the study region (Cruz et al., 2019).  
375 Additionally, Al, K, and Cl are linked to biomass burning (Reid et al., 1998; Reid et al., 2005;  
376 Schlosser et al., 2017; Wonaschütz et al., 2011). The source factor names should be interpreted  
377 with caution, as a single profile may consist of a mix of sources (e.g., waste processing). It  
378 should be noted that Cruz et al. (2019) performed PMF analysis for only the SWM18 season,  
379 which yielded similar and additional sources for only the SWM18 season, whereas this study  
380 used year-round data.

381 To provide size-resolved context for the five aerosol sources, Fig. 5 shows their respective  
382 reconstructed mass size distributions based on PMF output. Distributions for combustion,  
383 biomass burning, and waste processing primarily peaked in the submicrometer range, while  
384 crustal and sea salt sources primarily peaked in the supermicrometer range. Combustion and  
385 biomass burning factors showed a dominant peak between  $0.32 - 0.56 \mu\text{m}$ , whereas waste  
386 processing had a peak between  $0.56 - 1 \mu\text{m}$ . The crustal and sea salt factors exhibited their peak  
387 concentrations between  $1.8 - 5.6 \mu\text{m}$ . Both crustal and biomass burning sources showed signs of  
388 bimodal size distributions with a minor peak in the sub- and supermicrometer ranges,  
389 respectively.

390 As reported in Table 2, combustion was the largest contributor to the cumulative mass  
391 concentrations of organic acids and MSA, with the largest influence being for maleate (69.7 %)  
392 and MSA (57.4 %). Biomass burning was marked by its significant contribution to succinate  
393 (90.3 %). The sea salt source showed minor contributions to phthalate (9.9 %) and adipate (4.7  
394 %). The crustal source contributed appreciably to adipate (35.9 %) and oxalate (31.2 %), with the  
395 rest of the organic acid or MSA species being less influenced (0.1 – 13.3 %). Organic acids have  
396 been shown in past work to be associated with mineral dust (Russell et al., 2002), including both  
397 oxalic and adipic acids (Falkovich et al., 2004; Kawamura et al., 2013; Sullivan and Prather,  
398 2007; Tsai et al., 2014), although less has been documented for adipate. Wang et al. (2017) and  
399 Yao et al. (2003) both report that gaseous acids are likely to adsorb onto supermicrometer  
400 particles that are highly alkaline, such as dust. The waste processing factor contributed to  
401 maleate (30.1 %), oxalate (10.5 %), and MSA (1.4 %). An unexpected result was that the sea salt  
402 factor did not contribute to MSA even though the latter is derived from ocean-emitted DMS; the  
403 results of Table 2 suggest that other sources such as biomass burning and industrial activities are  
404 more influential in the study region similar to other regions like Beijing (Yuan et al., 2004) and  
405 coastal and inland areas of California (Sorooshian et al., 2015).

406

### 407 3.3 Species interrelationships

408 Correlation analysis was conducted for the same species used in the PMF analysis to quantify  
409 interrelationships and to gain additional insight into common production pathways. Correlation  
410 coefficients ( $r$ ) values are reported in Table 3 for for the sub- and supermicrometer ranges,



411 whereas results for full size range are shown in Table S6. Values are only shown and discussed  
412 subsequently for correlations with p-values below 0.05. Unless otherwise stated, correlations  
413 discussed below correspond to the full size range for simplicity, whereas notable results when  
414 contrasting the two size ranges ( $< 1 \mu\text{m}$  and  $> 1 \mu\text{m}$ ) are explicitly mentioned.

415 MSA exhibited a statistically significant correlation with Rb ( $r = 0.37$ ), suggestive of its link  
416 with biomass burning as Rb has been shown in the study region to be a biomass burning marker  
417 (Braun et al., 2020). Additionally, MSA was correlated with Na,  $\text{NO}_3^-$ , and  $\text{SO}_4^{2-}$  ( $r: 0.35 - 0.59$ ),  
418 which are associated with marine aerosol (e.g., sea salt, DMS, shipping) but also biomass  
419 burning. The supermicrometer results indicate MSA was correlated only with Na ( $r = 0.32$ ), due  
420 presumably to co-emission from both crustal and sea salt sources, with the former commonly  
421 linked to biomass burning (Schlosser et al., 2017). For the submicrometer range, MSA was  
422 correlated with Rb and  $\text{SO}_4^{2-}$  ( $r: 0.39 - 0.60$ ), which are derived from biomass burning and other  
423 forms of combustion, consistent with smaller particles formed secondarily from gas-to-particle  
424 conversion processes. That is also why MSA was well correlated with succinate, oxalate, and  
425 phthalate ( $r: 0.53 - 0.67$ ), which were also prominent species in either (or both of) the biomass  
426 burning and combustion factors.

427 Adipate only exhibited significant correlations with maleate and phthalate for the full diameter  
428 range ( $r: 0.43 - 0.45$ ), while maleate was correlated only with adipate. In contrast, succinate,  
429 oxalate, and phthalate were correlated with a wide suite of species, indicating that maleate and  
430 adipate exhibited more unique behavior in terms of their production routes. Succinate, oxalate,  
431 and phthalate similarly exhibited significant correlations with each other, and species linked to  
432 crustal sources (Al, Ti, Na), sea salt (Na), and biomass burning (Rb). Succinate and oxalate in  
433 particular were better correlated with tracer species related to either dust or sea salt (Al, Na) in  
434 the supermicrometer range, and were correlated with each other also in that size range.

435

#### 436 3.4 Cumulative size distribution variations

437 Mass size distributions for each individual organic acid and MSA are shown for the full study  
438 period in Fig. S2 and seasonal mass size distributions can be seen in Figs. 6-11. General  
439 information for the cumulative dataset will be described here before examining seasonal results  
440 in Sect. 4. While significant variability exists between individual sets for the cumulative dataset,  
441 a few general features are evident: (i) mass size distributions all appear multi-modal with the  
442 exception of maleate, which on average exhibited a uni-modal profile; (ii) all species show a  
443 larger peak in the submicrometer range versus supermicrometer sizes; (iii) phthalate and adipate  
444 show more comparable peaks in the sub- and supermicrometer range; and (iv) the size bin where  
445 the peaks occur vary between species. These results point to differences in the species with  
446 regard to their source, formation mechanism, and eventual fate.

447 One factor relevant to the mass size distribution plots is the source origin of sampled air masses.  
448 The WCWT plots in Fig. 12 reveal the bulk of the concentration of a few species (e.g., phthalate,  
449 succinate, and MSA) was explained by southwesterly flow. Consistent with the PMF results  
450 showing that the biomass burning factor contributed the most to these three species, the



451 predominant fire sources were to the southwest of Luzon. Past work has linked these areas to  
452 significant biomass burning influence over Luzon and the South China Sea during the SWM  
453 season (Atwood et al., 2017; Ge et al., 2017; Hilario et al., 2020b; Reid et al., 2016; Song et al.,  
454 2018; Wang et al., 2013; Xian et al., 2013). Noteworthy is that the WCWT maps for SWM18  
455 reveal more influence from the biomass burning hotspots to the southwest (e.g., Borneo and  
456 Sumatra), in contrast to SWM19, pointing to more biomass burning influence in the former  
457 season. Oxalate's WCWT profile shows the most spatial heterogeneity in terms of source  
458 regions; this is consistent with it being an end-product in the oxidation of other carboxylic acids  
459 that can originate from numerous sources. Finally, adipate and maleate similarly showed a  
460 localized hotspot in terms of where their greatest influence originated, approximately 290 km to  
461 the north-northwest of MO. This could be partly linked to the Sual coal-fired power station  
462 located near that area where an ash disposal site is also in close proximity. The uniquely similar  
463 WCWT maps between adipate and maleate is consistent with them having few correlations, if  
464 any, with species aside from each other (Table S6). Subsequent sections discuss each organic  
465 acid and MSA in more detail including seasonal behavior.

466

#### 467 **4. Discussion**

##### 468 **4.1 Phthalate**

469 Results from Sect. 3 show that phthalate has the following characteristics: (i) influenced most by  
470 biomass burning (49.5 %), followed by combustion (27.4 %), crustal sources (13.3 %), and then  
471 sea salt (9.9 %); (ii) significant correlations with more species in Table S6 than any other organic  
472 acid or MSA; (iii) comparable mass size distribution modes in the sub- and supermicrometer size  
473 ranges; (iv) highest mass concentration in the Trans period, but also exhibited significantly  
474 different concentrations between the two SWM seasons; and (v) had concentrations dominated  
475 by sources to the southwest. Previous studies measuring phthalate in other regions have found  
476 concentrations of 40.1 – 105 ng m<sup>-3</sup> (Hong Kong; PM<sub>2.5</sub>; Ho et al. (2006)), <0.01 – 7.6 ng m<sup>-3</sup>  
477 (remote marine; total suspended particles (TSP); Kawamura and Sakaguchi (1999)), 0.16 – 3.25  
478 ng m<sup>-3</sup> (Arctic; TSP; Kawamura et al. (2010)), and 0 – 57.3 ng m<sup>-3</sup> (Rondônia, Brazil; PM<sub>2.5</sub>;  
479 Decesari et al. (2006)). The latter was more consistent with concentrations in this study (0 –  
480 67.02 ng m<sup>-3</sup>), albeit the size ranges examined vary. A more detailed examination based on  
481 seasonally resolved mass size distributions and WCWT maps follows to try to gain more insights  
482 into this species. Although not referenced hereafter, Table S7 provides numerical details about  
483 mass concentration mode sizes and associated concentrations for each season and the cumulative  
484 dataset for each species.

485 The average size distributions for phthalate appeared bi-modal for each individual season (Fig.  
486 6). Depending on the season, concentration peaks occurred in three separate MOUDI stages for  
487 the submicrometer range, and between 1.8 – 3.2 or 3.2 – 5.6 μm in the supermicrometer range.  
488 The NEM season was unique in that the supermicrometer peak was considerably more  
489 pronounced than in the submicrometer range, which was a rare occurrence in this study for all  
490 species except adipate. Phthalate appears in the submicrometer range due to secondary formation



491 by photo-oxidation (i.e., Kautzman et al., 2010; Kawamura and Ikushima, 2002; Kawamura and  
492 Yasui, 2005; Kleindienst et al., 2012) and from primary emissions (i.e., combustion,  
493 biomass/waste burning) (i.e., Deshmukh et al., 2016; Kawamura and Kaplan, 1987; Kumar et al.,  
494 2015; Kundu et al., 2010). Its general presence in the supermicrometer range, especially during  
495 the NEM season, can be explained by possible adsorption onto larger particles such as dust and  
496 sea salt (i.e., Wang et al., 2012; Wang et al., 2017). Others have observed an enhancement in  
497 phthalate in the supermicrometer mode, specifically in Xi'an, China, due to suspected adsorption  
498 of its vapor form (Wang et al., 2012) derived from photo-oxidation of naphthalene (Ho et al.,  
499 2006; Wang et al., 2011; Wang et al., 2012; Wang et al., 2017).

500 WCWT results for phthalate (Fig. S3) showed high concentrations across all seasons coming  
501 from the southwest, most notably in the SWM18 and SWM19 seasons. The significant reduction  
502 in phthalate levels from SWM18 ( $16.75 \pm 24.80 \text{ ng m}^{-3}$ ) to SWM19 ( $5.72 \pm 7.41 \text{ ng m}^{-3}$ ) is  
503 coincident with stronger influence from biomass burning from the southwest in 2018. Figure 3  
504 showed that the highest concentration of phthalate occurred in the Trans period, assumed to be  
505 largely due to local emissions (e.g., vehicular traffic) based on the WCWT results with  
506 significant influence in the immediate vicinity of Luzon unlike the other seasons. The peculiar  
507 size distribution results for the NEM season can be explained by the WCWT map showing  
508 strong influence from the northeast, which likely includes supermicrometer aerosol influences  
509 from sea salt and dust from East Asia. The reduced influence of upwind anthropogenic and  
510 biomass burning emissions during the NEM season can explain the lower seasonal  
511 concentrations, especially in the submicrometer size range (Hsu et al., 2009).

512

#### 513 4.2 Adipate

514 Adipate was shown in Sect. 3 to have the following features: (i) influenced most by crustal  
515 sources (35.9 %), followed by combustion (32.9 %), biomass burning (26.4 %), and finally sea  
516 salt (4.7 %); (ii) only correlated with maleate and phthalate; (iii) comparable concentrations in  
517 the sub- and supermicrometer size ranges, with a mode between 5.6 and 10  $\mu\text{m}$ ; (iv) highest mass  
518 concentration in the SWM seasons, but especially the SWM19 season; and (v) concentrations  
519 dominated by sources from the southwest as well as from the northwest. Concentrations for  
520 adipate measured in other regions include 3.78 – 32.1  $\text{ng m}^{-3}$  (Hong Kong;  $\text{PM}_{2.5}$ ; Ho et al.  
521 (2006)), 3.8 – 16.8  $\text{ng m}^{-3}$  (Rondônia, Brazil;  $\text{PM}_{2.5}$ ; Decesari et al. (2006)), 0.60 – 13  $\text{ng m}^{-3}$   
522 (remote marine; TSP; Kawamura and Sakaguchi (1999)) and 0.21 – 2.94  $\text{ng m}^{-3}$  (Arctic; TSP;  
523 Kawamura et al. (2010)). The range in this study was 0 – 43.83  $\text{ng m}^{-3}$ , with an upper bound that  
524 exceeded those in the previous works.

525 Mass size distributions for adipate were the most variable in structure compared to the other five  
526 species with multiple peaks present at different sizes (Fig. S2). In general, its distributions  
527 appeared uniquely and consistently tri-modal with the exception of the SWM18 season where it  
528 was bi-modal (Fig. 7). Modes appeared between 0.10 – 0.18  $\mu\text{m}$  and 0.32 – 0.56  $\mu\text{m}$  for the  
529 submicrometer range, and between 1.0 – 1.8  $\mu\text{m}$  and 3.2 – 5.6  $\mu\text{m}$  in the supermicrometer range.  
530 The SWM19 season was unique for adipate as the highest peak was in the supermicrometer



531 range and it was higher than any other peak across the other seasons. Submicrometer adipate is  
532 likely derived from a photo-oxidation of higher chain organic acids (i.e., van Drooge and  
533 Grimalt, 2015), ozonolysis of vehicular emissions (i.e., Grosjean et al., 1978), and from the  
534 primary emissions of biomass burning (i.e., Graham et al., 2002). The appearance in the  
535 supermicrometer range likely due to adsorption onto larger particles such as dust and sea salt  
536 (e.g., Wang et al., 2012; Wang et al., 2017). As the PMF results suggest crustal sources were  
537 more influential for adipate in contrast to sea salt, dust was more likely the supermicrometer  
538 particle type that adipate preferentially partitioned to. The source of the dust was likely a  
539 combination of long-range transport from (i) the southwest especially during biomass burning  
540 periods, (ii) East Asia, and (iii) locally generated dust via anthropogenic activities (Fig. S4).

541 Past work in the study region showed that broad mass size distributions with comparable  
542 concentrations in the sub- and supermicrometer ranges were coincident with wet scavenging  
543 (Braun et al., 2020) and appreciable primary emissions of sea salt and dust (AzadiAghdam et al.,  
544 2019; Cruz et al., 2019). Scavenging was suggested to remove transported pollution while  
545 allowing for more pronounced contributions from more localized emissions, which could include  
546 vehicular traffic, sea salt, and anthropogenic forms of dust (e.g., road dust, construction), all of  
547 which are consistent with adipate's mass size distribution data and WCWT maps (Fig. S4)  
548 showing high concentrations predominately around Luzon for all seasons.

549

#### 550 4.3 Succinate

551 Succinate exhibited the following characteristics: (i) influenced primarily by biomass burning  
552 (90.3 %) followed by crustal sources (9.7 %); (ii) exhibited high correlation coefficients (0.67 –  
553 0.76) with oxalate, phthalate, and MSA (Table S6); (iii) mass was focused in the submicrometer  
554 range; (iv) highest mass concentrations were in the SWM18 season, and, similar to phthalate,  
555 showed a significant reduction in the SWM19 season; and (v) had concentrations dominated by  
556 sources from the southwest. The range of concentrations in this study (0 – 166.28 ng m<sup>-3</sup>) is  
557 somewhat consistent with those from other regions: 61.8 – 261 ng m<sup>-3</sup> (Rondônia, Brazil; PM<sub>2.5</sub>;  
558 Decesari et al. (2006)), 13.1 – 121 ng m<sup>-3</sup> (Hong Kong; PM<sub>2.5</sub>; Ho et al. (2006)), 9.2 – 31.7 ng m<sup>-3</sup>  
559 (New England, USA; 0.4 – 10 μm; Ziemba et al. (2011)), 0.29 – 16 ng m<sup>-3</sup> (Remote Marine;  
560 TSP; Kawamura and Sakaguchi (1999)), and 1.35 – 12.9 ng m<sup>-3</sup> (Arctic; TSP; Kawamura et al.  
561 (2010)).

562 The average size distributions for succinate varied in the number of peaks present (2 – 4), but on  
563 average were bi-modal with a submicrometer mode usually between 0.32 – 0.56 μm or 0.56 – 1.0  
564 μm, and a smaller supermicrometer mode between either 1.8 – 3.2 μm or 3.2 – 5.6 μm (Fig. 8).  
565 The chief source of succinate, which is concentrated in the submicrometer peak, is biomass  
566 burning (Pratt et al., 2011; Vasconcellos et al., 2010), which is reinforced by the PMF results  
567 (Table 2), its high correlation with the biomass burning tracer Rb (r = 0.67; Table S6) (Braun et  
568 al., 2020) and WCWT maps showing its most pronounced influence from biomass burning  
569 hotspots to the southwest during the SWM18 season (Fig. S5). There likely was also local  
570 biomass burning during the NEM season contributing to succinate concentrations. Hilario et al.



571 (2020a) showed based on satellite data that local fire activity peaks between March and May.  
572 There was less influence from biomass burning in the SWM19 season, which is why succinate's  
573 levels were lower ( $4.73 \pm 7.43 \text{ ng m}^{-3}$ ) than in the SWM18 season ( $21.61 \pm 43.10 \text{ ng m}^{-3}$ ).  
574 Similar to phthalate and adipate, there were more local hotspots of concentration in seasonal  
575 WCWT maps pointing to local anthropogenic sources such as vehicular traffic and the presence  
576 of supermicrometer particles like dust and sea salt that succinate can partition to (e.g., Wang et  
577 al., 2012; Wang et al., 2017).

578

#### 579 4.4 Maleate

580 The results of Sect. 3 showed that maleate had the following attributes: (i) influenced most by  
581 combustion (69.7 %), followed by waste processing (30.1 %), and then barely by crustal sources  
582 (0.2 %); (ii) only correlated with adipate of all species shown in Table S6; (iii) showed a uni-  
583 modal mass size distribution, with negligible contribution in the supermicrometer range; (iv)  
584 highest mass concentration in the SWM19 season, but was comparable to the SWM18 season;  
585 and (v) WCWT maps showed the most localized sources as compared to the other species  
586 examined (Fig. 11). Maleate concentrations have been reported for other regions as follows: 7 –  
587  $75 \text{ ng m}^{-3}$  (Rondônia, Brazil;  $\text{PM}_{2.5}$ ; Decesari et al. (2006)),  $2.21 - 37.2 \text{ ng m}^{-3}$  (Hong Kong;  
588  $\text{PM}_{2.5}$ ; Ho et al. (2006)),  $4.9 - 9.2 \text{ ng m}^{-3}$  (New England, USA;  $0.4 - 10 \mu\text{m}$ ; Ziembra et al.  
589 (2011)),  $0.04 - 3.8 \text{ ng m}^{-3}$  (remote marine; TSP; Kawamura and Sakaguchi (1999)), and  $0.04 -$   
590  $0.83 \text{ ng m}^{-3}$  (Arctic; TSP; Kawamura et al. (2010)). The values reported for this study region  
591 tended to be higher ( $0-119.19 \text{ ng m}^{-3}$ ), which is unsurprising as vehicular emissions are so  
592 prominent in the Metro Manila region (Alas et al., 2018; Kecorius et al., 2017).

593 The average seasonal size distributions for maleate appeared to be uni-modal with peaks between  
594  $0.32 - 0.56 \mu\text{m}$  and  $0.56 - 1.0 \mu\text{m}$  (Fig. 9). The absence of a supermicrometer peak, in contrast to  
595 most other species, indicates that it had less diverse sources and was derived from combustion  
596 emissions without being adsorbed onto supermicrometer particles like the other species  
597 investigated. The association of maleate with the waste processing source factor in Table 2 can  
598 be explained partly by the burning and recycling of electronic waste (Cruz et al., 2019; Gullett et  
599 al., 2007; Iijima et al., 2007). The Pabroa et al. (2011) study reported that there are few licensed  
600 operators for battery recycling, but there are numerous unregulated melters frequently melting  
601 metal and discarding the waste.

602 Seasonal WCWT maps for maleate (Fig. S6) consistently showed hotspots around Luzon  
603 indicative of local emissions. Maleate concentrations for the SWM18 ( $18.68 \pm 14.89 \text{ ng m}^{-3}$ ) and  
604 SWM19 ( $19.44 \pm 34.04 \text{ ng m}^{-3}$ ) were significantly higher than the other seasons (Trans:  $3.81 \pm$   
605  $4.23 \text{ ng m}^{-3}$ ; NEM:  $1.65 \pm 3.65 \text{ ng m}^{-3}$ ), and this could likely be due to increased traffic  
606 emissions because of gridlock due to intense rainfall. It should be noted that the Ateneo de  
607 Manila campus has student break periods in March, April, May, and December (Hilario et al.,  
608 2020a); those months pertain to the NEM season, which could lead to lower combustion  
609 emissions from vehicles (e.g., maleate and phthalate). Although the SWM season is associated  
610 with enhanced precipitation over Metro Manila, lower boundary layer height and appreciable RH



611 values could counteract wet scavenging to some degree by promoting aqueous processing of  
612 aerosol (Hilario et al., 2020a). Furthermore, maleate's largely submicrometer size distribution  
613 (Fig. 9) may reduce the efficiency of wet scavenging (Greenfield, 1957).

614

#### 615 4.5 Oxalate

616 Oxalate was shown to have the following traits: (i) influenced somewhat uniformly by  
617 combustion (32.9 %) and crustal (31.2 %) sources, followed by biomass burning (25.4 %), and  
618 waste processing (10.5 %); (ii) only organic acid to correlate with combustion tracers (V, Ni);  
619 (iii) pronounced presence in both the sub- and supermicrometer size ranges; (iv) highest mass  
620 concentrations in the Trans period; and (v) had contributions from the southwest, east/northeast,  
621 and locally. Oxalate concentrations in this study ( $148.59 \pm 94.26 \text{ ng m}^{-3}$ ) were surprisingly low  
622 for such a polluted megacity with strong regional sources. For context, concentrations in a few  
623 other regions are as follows:  $1.14 \mu\text{g m}^{-3}$  in Sao Paulo, Brazil (Souza et al., 1999);  $0.27 - 1.35 \mu\text{g}$   
624  $\text{m}^{-3}$  in Tokyo, Japan (Kawamura and Ikushima, 2002; Sempère and Kawamura, 1994);  $0.49 \mu\text{g}$   
625  $\text{m}^{-3}$  in Los Angeles, California (Kawamura et al., 1985);  $220 - 300 \text{ ng m}^{-3}$  in Nanjing, China  
626 (Yang et al., 2005);  $75 - 210 \text{ ng m}^{-3}$  for multiple sites in Europe (Hungary, Belgium, Finland)  
627 (Maenhaut et al., 2011);  $12.3 - 33.7 \text{ ng m}^{-3}$  in Cape San Juan, Puerto Rico (Jusino-Atresino et  
628 al., 2016);  $20 - 400 \text{ ng m}^{-3}$  in rural/urban Finland (Kerminen et al., 2000); and  $1 - 42 \text{ ng m}^{-3}$   
629 around the Atlantic Ocean/Antarctic (Virkkula et al., 2006).

630 The average size distributions for oxalate appeared bi-modal for each individual season with  
631 modes between  $0.32 - 0.56 \mu\text{m}$  and  $0.56 - 1.0 \mu\text{m}$  for the submicrometer range and a separate  
632 mode between  $1.8 - 3.2 \mu\text{m}$  for the supermicrometer range (Fig. 10). A unique aspect for oxalate  
633 was its consistency in having a bi-modal profile each season with the supermicrometer mode  
634 always between  $1.8 - 3.2 \mu\text{m}$ . Submicrometer oxalate likely originated from secondary  
635 production from both biogenic and anthropogenic precursor emissions, and potentially from  
636 primary emissions (i.e., combustion/biomass burning) (i.e., Decesari et al., 2006; Falkovich et  
637 al., 2005; Golly et al., 2019; Kundu et al., 2010; Wang et al., 2010). Of all the six species  
638 studied, oxalate was best correlated with  $\text{SO}_4^{2-}$  ( $r = 0.69$ ; Table S6), especially in the  
639 submicrometer range ( $r = 0.72$ ; Table 3), which is consistent with their common production  
640 mechanism via aqueous processing (Sorooshian et al., 2006; Yu et al., 2005). Additionally, high  
641 concentrations of oxalate in the Trans period indicate that photo-oxidation was an important  
642 process for oxalate formation since the Trans period had low rain and high solar radiation. The  
643 prominent supermicrometer presence was likely due to adsorption onto supermicrometer  
644 particles. Past work by Sullivan and Prather (2007) reported the following with regard to  
645 oxalate's behavior in coarse particles of relevance to this study: (i) oxalic acid was  
646 predominately associated with mineral dust and to a lesser degree with aged sea salt; (ii) even  
647 though most of the total mass was sea salt, there was more oxalate per mass of mineral dust than  
648 sea salt; (iii) Asian dust particles are more alkaline as opposed to sea salt and therefore act as  
649 better sinks for dicarboxylic acids than sea salt; and (iv) it is feasible that a large fraction of  
650 supermicrometer dicarboxylic acid mass in remote marine air is associated with mineral dust and  
651 not sea salt. The PMF results from the present study indicate that oxalate was much more



652 influenced by crustal sources (31.2 %) versus sea salt (0 %), similar to phthalate, adipate, and  
653 succinate (Table 2). Reinforcing the relationship between oxalate and dust is the significant  
654 correlation between oxalate and both Al ( $r = 0.59$ ) and Ti (0.29) in the supermicrometer range.

655 WCWT results for oxalate (Fig. S7) showed high concentrations around Luzon for all seasons,  
656 with the caveat that the SWM18 exhibited high concentrations coming from the southwest,  
657 which has already been linked to biomass burning emissions. The difference in oxalate levels  
658 between the SWM18 ( $177.86 \pm 139.41 \text{ ng m}^{-3}$ ) and SWM19 ( $110.21 \pm 62.06 \text{ ng m}^{-3}$ ) seasons is  
659 largely due to the enhanced contribution of biomass burning in the former season since oxalate is  
660 abundant in fire emissions (Falkovich et al., 2005; Mardi et al., 2018; Narukawa et al., 1999).

661

#### 662 4.6 MSA

663 Previous sections revealed the following characteristics for MSA: (i) influenced most by  
664 combustion (57.4 %), followed by biomass burning (41.2 %), waste processing (1.4 %), and then  
665 crustal sources (0.1 %); (ii) significantly correlated with succinate, oxalate, phthalate, and  $\text{SO}_4^{2-}$ ;  
666 (iii) similar to maleate, primarily consisted of a submicrometer mass size distribution peak with  
667 only minor contributions from the supermicrometer mode; (iv) concentration was highest during  
668 the SWM18 season; and (v) had concentrations dominated by sources from the southwest.  
669 Concentrations of MSA in this study were surprisingly low for a site so close to marine and  
670 anthropogenic sources ( $0.10 - 23.23 \text{ ng m}^{-3}$ ). For context, MSA concentrations in other regions  
671 are as follows: 30-60  $\text{ng m}^{-3}$  in Nanjing, China (Yang et al., 2005); 29 – 79  $\text{ng m}^{-3}$  for multiple  
672 sites in Europe (Hungary, Belgium, Finland) (Maenhaut et al., 2011); 2.33 – 3.33  $\text{ng m}^{-3}$  in  
673 Cape San Juan, Puerto Rico (Jusino-Atresino et al., 2016); 5 – 115  $\text{ng m}^{-3}$  in rural/urban Finland  
674 (Kerminen et al., 2000); 2.8 – 20  $\text{ng m}^{-3}$  around the Atlantic Ocean/Antarctic (Virkkula et al.,  
675 2006); ~7  $\text{ng m}^{-3}$  in Tucson, Arizona and ~101  $\text{ng m}^{-3}$  Marina, California (Sorooshian et al.,  
676 2015); 29 – 66  $\text{ng m}^{-3}$  over the China Sea (Gao et al., 1996); 13 – 59  $\text{ng m}^{-3}$  at various coastal  
677 and island sites over the North Pacific Ocean (Arimoto et al., 1996); and  $34 \pm 33 \text{ ng m}^{-3}$  over  
678 Houston, Texas (Sorooshian et al., 2007b).

679 The average size distributions for MSA appeared uni-modal with the peak size being between  
680  $0.32 - 0.56 \mu\text{m}$  (Fig. 11). The consistent mass size distribution for MSA in all seasons, similar to  
681 maleate, could be due to some combination of limited sources and production pathways.  
682 Surprisingly, MSA showed no association to the sea salt source factor (Table 2) even though it  
683 would be expected given that DMS is co-emitted from the ocean with sea salt. Instead,  
684 combustion and biomass burning sources were more significant, which is consistent with some  
685 past studies linking MSA to anthropogenic sources (Yuan et al., 2004) and biomass burning  
686 (Sorooshian et al., 2015). WCWT results for MSA (Fig. S8) showed high concentrations coming  
687 from the southwest during the SWM18 and SWM19 seasons, and from the east-northeast during  
688 the NEM and Trans period.

689

#### 690 4. Conclusions



691 This work used a 16-month long dataset of size-resolved aerosol composition to investigate the  
692 nature of five organic acids (oxalate, succinate, adipate, maleate, and phthalate) and MSA in the  
693 polluted Metro Manila region in the Philippines. Selected results are as follows in order of the  
694 three major questions posed at the end of Sect. 1.

- 695 • Organic acids and MSA contribute only a small fraction to the total gravimetric aerosol  
696 mass in Metro Manila ( $0.80 \pm 0.66$  %). The combined contribution of these six species  
697 was similar between the sub- and supermicrometer range (0.78 % and 0.84 %,  
698 respectively). After accounting for water-soluble ions and elements, and black carbon,  
699 there still was an unresolved mass fraction amounting to 33.74 % across all sizes, and  
700 17.78 % and 69.10 % for sub- and supermicrometer sizes, respectively. Therefore, future  
701 work is still warranted to identify what the missing fraction is comprised of, which is  
702 speculated to be water-insoluble organics and elements.
- 703 • Oxalate was the most abundant of the six species accounting for 69.1 – 87.3 % of the  
704 total combined mass of the six species depending on the season. However, the bulk  
705 concentrations of oxalate were unusually low ( $148.59 \pm 94.26$  ng m<sup>-3</sup>) for such a polluted  
706 area in contrast to other populated regions. Concentrations of the other five species were  
707 much lower than oxalate, with mean levels for the entire study period being less than 10  
708 ng m<sup>-3</sup>. In particular, MSA exhibited the lowest mean concentration ( $5.40 \pm 5.23$  ng m<sup>-3</sup>).  
709 It is unclear exactly as to the reason for the low concentrations of the examined species in  
710 light of the diverse marine and anthropogenic sources in the region. The role of wet  
711 scavenging, especially in the SWM seasons, will be the subject of future research.
- 712 • The six species exhibited different behavior seasonally, both in terms of relative  
713 concentration and mass size distribution. The SWM18 season was uniquely different than  
714 the SWM19 season, owing to more biomass burning emissions transported from the  
715 southwest that yielded enhanced levels for most species in the submicrometer range,  
716 especially succinate, MSA, oxalate, and phthalate. Enhanced precipitation in the SWM  
717 seasons also was coincident with more influence from localized emissions leading to  
718 enhanced levels in the sub- and supermicrometer ranges depending on the species. The  
719 NEM season was characterized by generally lower concentrations of most species as air  
720 was predominantly transported from the northeast with reduced influence of  
721 anthropogenic and biomass burning emissions. Phthalate was enhanced in the  
722 supermicrometer range during the NEM season due to presumed adsorption to Asian dust  
723 and to a lesser extent sea salt. The Trans season was characterized by having strong  
724 influence from localized emissions for all six species, which promoted especially high  
725 concentrations for phthalate and oxalate in both the sub- and supermicrometer ranges.
- 726 • All species exhibited a prominent submicrometer peak that likely stemmed largely from  
727 secondary formation from both anthropogenic and biogenic precursor emissions and was  
728 especially prominent during the SWM18 season due to extensive biomass burning  
729 influence. Biomass burning was an especially important source for succinate, phthalate,  
730 MSA, oxalate, and adipate. All six species exhibited relatively low association with sea  
731 salt particles; this was particularly interesting for MSA, which was instead better related  
732 to combustion and biomass burning emissions. In contrast to sea salt, most species were



733 linked to crustal emissions as evident from peaks in the coarse mode during periods of  
734 dust influence. Oxalate, adipate, phthalate, and succinate in particular preferentially  
735 partitioned to dust rather than sea salt, potentially due to their affinity for alkaline particle  
736 types. Oxalate was best correlated with sulfate, especially in the submicrometer mode,  
737 explained by their common production via aqueous processing, which is common in the  
738 study region owing to high humidity levels year-round.

739 The results of this study point to the importance of size-resolved measurements of organic and  
740 sulfonic acids as this extensive dataset revealed important changes in mass size distributions  
741 between species and for different seasons. The data point to the partitioning of these species to  
742 coarse aerosol types and the potentially significant impact of precipitation on either the removal  
743 or enhancement of species' mass size distribution modes; these topics warrant additional  
744 research to put on firmer ground the sensitivity of these species to source regions, transport  
745 pathway, and wet scavenging effects. More research is warranted to investigate the remaining  
746 fraction of the unresolved mass (approximately one third of the gravimetric mass) that is not  
747 accounted for by black carbon and the water-soluble constituents speciated in this work. This is  
748 especially important for the supermicrometer range. Lastly, the current results point to the  
749 question as to what drives the affinity of individual species towards the coarse mode for different  
750 aerosol types (e.g., dust, sea salt), and how common this is for other regions.

751

#### 752 **Data availability**

753 Size-resolved aerosol data collected at Manila Observatory are described in Stahl et al. (2020b)  
754 and archived on figshare (Stahl et al., 2020a) as well as on the NASA data repository at  
755 DOI:10.5067/Suborbital/CAMP2EX2018/DATA001.

756

#### 757 **Author contribution**

758 MTC, MOC, JBS, RAB, ABM, CS, and AS designed the experiment. All coauthors carried out  
759 various aspects of the data collection. MTC, RAB, CS, and AS conducted analysis and  
760 interpretation of the data. CS and AS prepared the manuscript with contributions from the  
761 coauthors.

762

#### 763 **Competing interests**

764 The authors declare that they have no conflict of interest.

765

#### 766 **Acknowledgements**

767 The authors acknowledge support from NASA grant 80NSSC18K0148 in support of the NASA  
768 CAMP<sup>2</sup>Ex project. R. A. Braun acknowledges support from the ARCS Foundation. Cruz



769 acknowledges support from the Philippine Department of Science and Technology's ASTHRD  
770 Program. A. B. MacDonald acknowledges support from the Mexican National Council for  
771 Science and Technology (CONACYT). We acknowledge Agilent Technologies for their support  
772 and Shane Snyder's laboratories for ICP-QQQ data.

773

#### 774 **References**

- 775 Adam, M. G., Chiang, A. W. J., and Balasubramanian, R.: Insights into characteristics of light  
776 absorbing carbonaceous aerosols over an urban location in Southeast Asia, *Environ Pollut*, 257,  
777 113425, 10.1016/j.envpol.2019.113425, 2020.
- 778 Agarwal, R., Shukla, K., Kumar, S., Aggarwal, S. G., and Kawamura, K.: Chemical composition  
779 of waste burning organic aerosols at landfill and urban sites in Delhi, *Atmos Pollut Res*, 11, 554-  
780 565, 10.1016/j.apr.2019.12.004, 2020.
- 781 Akasaka, I., Morishima, W., and Mikami, T.: Seasonal march and its spatial difference of rainfall  
782 in the Philippines, *Int J Climatol*, 27, 715-725, 10.1002/joc.1428, 2007.
- 783 Alas, H. D., Müller, T., Birmili, W., Kecorius, S., Cambaliza, M. O., Simpas, J. B. B., Cayetano,  
784 M., Weinhold, K., Vallar, E., Galvez, M. C., and Wiedensohler, A.: Spatial Characterization of  
785 Black Carbon Mass Concentration in the Atmosphere of a Southeast Asian Megacity: An Air  
786 Quality Case Study for Metro Manila, Philippines, *Aerosol Air Qual Res*, 18, 2301-2317,  
787 10.4209/aaqr.2017.08.0281, 2018.
- 788 Allen, A. G., Nemitz, E., Shi, J. P., Harrison, R. M., and Greenwood, J. C.: Size distributions of  
789 trace metals in atmospheric aerosols in the United Kingdom, *Atmos Environ*, 35, 4581-4591,  
790 10.1016/s1352-2310(01)00190-x, 2001.
- 791 Allen, H. C., Laux, J. M., Vogt, R., Finlayson-Pitts, B. J., and Hemminger, J. C.: Water-Induced  
792 Reorganization of Ultrathin Nitrate Films on NaCl: Implications for the Tropospheric Chemistry  
793 of Sea Salt Particles, *J Phys Chem*, 100, 6371-6375, 10.1021/jp953675a, 1996.
- 794 Andreae, M. O.: Soot carbon and excess fine potassium: long-range transport of combustion-  
795 derived aerosols, *Science*, 220, 1148-1151, 10.1126/science.220.4602.1148, 1983.
- 796 Andreae, M. O., and Crutzen, P. J.: Atmospheric Aerosols: Biogeochemical Sources and Role in  
797 Atmospheric Chemistry, *Science*, 276, 1052-1058, 10.1126/science.276.5315.1052, 1997.
- 798 Arimoto, R., Duce, R. A., Savoie, D. L., Prospero, J. M., Talbot, R., Cullen, J. D., Tomza, U.,  
799 Lewis, N. F., and Ray, B. J.: Relationships among aerosol constituents from Asia and the North  
800 Pacific during PEM-West A, *J Geophys Res-Atmos*, 101, 2011-2023, 10.1029/95jd01071, 1996.
- 801 Artaxo, P., Gerab, F., Yamasoe, M. A., and Martins, J. V.: Fine mode aerosol composition at  
802 three long-term atmospheric monitoring sites in the Amazon Basin, *J Geophys Res*, 99, 22857-  
803 22868, 10.1029/94jd01023, 1994.
- 804 Asmi, E., Frey, A., Virkkula, A., Ehn, M., Manninen, H. E., Timonen, H., Tolonen-Kivimäki, O.,  
805 Aurela, M., Hillamo, R., and Kulmala, M.: Hygroscopicity and chemical composition of  
806 Antarctic sub-micrometre aerosol particles and observations of new particle formation, *Atmos  
807 Chem Phys*, 10, 4253-4271, 10.5194/acp-10-4253-2010, 2010.
- 808 Atwood, S. A., Reid, J. S., Kreidenweis, S. M., Blake, D. R., Jonsson, H. H., Lagrosas, N. D.,  
809 Xian, P., Reid, E. A., Sessions, W. R., and Simpas, J. B.: Size-resolved aerosol and cloud  
810 condensation nuclei (CCN) properties in the remote marine South China Sea – Part 1:  
811 Observations and source classification, *Atmos Chem Phys*, 17, 1105-1123, 10.5194/acp-17-  
812 1105-2017, 2017.



- 813 AzadiAghdam, M., Braun, R. A., Edwards, E.-L., Bañaga, P. A., Cruz, M. T., Betito, G.,  
814 Cambaliza, M. O., Dadashazar, H., Lorenzo, G. R., Ma, L., MacDonald, A. B., Nguyen, P.,  
815 Simpas, J. B., Stahl, C., and Sorooshian, A.: On the nature of sea salt aerosol at a coastal  
816 megacity: Insights from Manila, Philippines in Southeast Asia, *Atmos Environ*, 216, 116922,  
817 10.1016/j.atmosenv.2019.116922, 2019.
- 818 Baboukas, E. D., Kanakidou, M., and Mihalopoulos, N.: Carboxylic acids in gas and particulate  
819 phase above the Atlantic Ocean, *J Geophys Res-Atmos*, 105, 14459-14471,  
820 10.1029/1999jd900977, 2000.
- 821 Bagtasa, G., Cayetano, M. G., and Yuan, C.-S.: Seasonal variation and chemical characterization  
822 of PM<sub>2.5</sub> in northwestern Philippines, *Atmos Chem Phys*, 18, 4965-4980, 10.5194/acp-18-4965-  
823 2018, 2018.
- 824 Bagtasa, G., Cayetano, M. G., Yuan, C.-S., Uchino, O., Sakai, T., Izumi, T., Morino, I., Nagai,  
825 T., Macatangay, R. C., and Velazco, V. A.: Long-range transport of aerosols from East and  
826 Southeast Asia to northern Philippines and its direct radiative forcing effect, *Atmos Environ*,  
827 218, 117007, 10.1016/j.atmosenv.2019.117007, 2019.
- 828 Bagtasa, G., and Yuan, C.-S.: Influence of local meteorology on the chemical characteristics of  
829 fine particulates in Metropolitan Manila in the Philippines, *Atmos Pollut Res*, 11, 1359-1369,  
830 10.1016/j.apr.2020.05.013, 2020.
- 831 Bañares, E. N., Narisma, G. T. T., Simpas, J. B. B., Cruz, F. A. T., Lorenzo, G. R. H.,  
832 Cambaliza, M. O., and Coronel, R. C.: Diurnal characterization of localized convective rain  
833 events in urban Metro Manila, Philippines, *AGUFM*, 2018, A11J-2367, 2018.
- 834 Barbaro, E., Padoan, S., Kirchgeorg, T., Zangrando, R., Toscano, G., Barbante, C., and  
835 Gambaro, A.: Particle size distribution of inorganic and organic ions in coastal and inland  
836 Antarctic aerosol, *Environ Sci Pollut Res Int*, 24, 2724-2733, 10.1007/s11356-016-8042-x, 2017.
- 837 Bardouki, H., Berresheim, H., Vrekoussis, M., Sciare, J., Kouvarakis, G., Oikonomou, K.,  
838 Schneider, J., and Mihalopoulos, N.: Gaseous (DMS, MSA, SO<sub>2</sub>, H<sub>2</sub>SO<sub>4</sub> and DMSO) and  
839 particulate (sulfate and methanesulfonate) sulfur species over the northeastern coast of Crete,  
840 *Atmos Chem Phys*, 3, 1871-1886, 10.5194/acp-3-1871-2003, 2003a.
- 841 Bardouki, H., Liakakou, H., Economou, C., Sciare, J., Smolik, J., Ždímal, V., Eleftheriadis, K.,  
842 Lazaridis, M., Dye, C., and Mihalopoulos, N.: Chemical composition of size-resolved  
843 atmospheric aerosols in the eastern Mediterranean during summer and winter, *Atmos Environ*,  
844 37, 195-208, 10.1016/s1352-2310(02)00859-2, 2003b.
- 845 Bates, T. S., Lamb, B. K., Guenther, A., Dignon, J., and Stoiber, R. E.: Sulfur emissions to the  
846 atmosphere from natural sources, *J Atmos Chem*, 14, 315-337, 10.1007/bf00115242, 2004.
- 847 Bautista, A. T., Pabroa, P. C. B., Santos, F. L., Racho, J. M. D., and Quirit, L. L.: Carbonaceous  
848 particulate matter characterization in an urban and a rural site in the Philippines, *Atmos Pollut*  
849 *Res*, 5, 245-252, 10.5094/apr.2014.030, 2014.
- 850 Beaver, M. R., Garland, R. M., Hasenkopf, C. A., Baynard, T., Ravishankara, A. R., and Tolbert,  
851 M. A.: A laboratory investigation of the relative humidity dependence of light extinction by  
852 organic compounds from lignin combustion, *Environ Res Lett*, 3, 045003, 10.1088/1748-  
853 9326/3/4/045003, 2008.
- 854 Berresheim, H.: Biogenic sulfur emissions from the Subantarctic and Antarctic Oceans, *J*  
855 *Geophys Res*, 92, 13245-13262, 10.1029/JD092iD11p13245, 1987.
- 856 Bikkina, S., Kawamura, K., Miyazaki, Y., and Fu, P.: High abundances of oxalic, azelaic, and  
857 glyoxylic acids and methylglyoxal in the open ocean with high biological activity: Implication



- 858 for secondary OA formation from isoprene, *Geophys Res Lett*, 41, 3649-3657,  
859 10.1002/2014gl059913, 2014.
- 860 Biona, J. B., Mejia, A., Tacderas, M., Cruz, N. D., Dematera, K., and Romero, J.: Alternative  
861 Technologies for the Philippine Utility Jeepney A COST-BENEFIT STUDY, 2017.
- 862 Blando, J. D., and Turpin, B. J.: Secondary organic aerosol formation in cloud and fog droplets:  
863 a literature evaluation of plausibility, *Atmos Environ*, 34, 1623-1632, 10.1016/s1352-  
864 2310(99)00392-1, 2000.
- 865 Braun, R. A., Aghdam, M. A., Bañaga, P. A., Betito, G., Cambaliza, M. O., Cruz, M. T.,  
866 Lorenzo, G. R., MacDonald, A. B., Simpas, J. B., Stahl, C., and Sorooshian, A.: Long-range  
867 aerosol transport and impacts on size-resolved aerosol composition in Metro Manila, Philippines,  
868 *Atmos Chem Phys*, 20, 2387-2405, 10.5194/acp-20-2387-2020, 2020.
- 869 Brown, S. G., Eberly, S., Paatero, P., and Norris, G. A.: Methods for estimating uncertainty in  
870 PMF solutions: examples with ambient air and water quality data and guidance on reporting  
871 PMF results, *Sci Total Environ*, 518-519, 626-635, 10.1016/j.scitotenv.2015.01.022, 2015.
- 872 Cai, C., Marsh, A., Zhang, Y. H., and Reid, J. P.: Group Contribution Approach To Predict the  
873 Refractive Index of Pure Organic Components in Ambient Organic Aerosol, *Environ Sci*  
874 *Technol*, 51, 9683-9690, 10.1021/acs.est.7b01756, 2017.
- 875 Carlton, A. G., Turpin, B. J., Lim, H.-J., Altieri, K. E., and Seitzinger, S.: Link between isoprene  
876 and secondary organic aerosol (SOA): Pyruvic acid oxidation yields low volatility organic acids  
877 in clouds, *Geophys Res Lett*, 33, 10.1029/2005gl025374, 2006.
- 878 Chebbi, A., and Carlier, P.: Carboxylic acids in the troposphere, occurrence, sources, and sinks:  
879 A review, *Atmos Environ*, 30, 4233-4249, 10.1016/1352-2310(96)00102-1, 1996.
- 880 Chow, J. C., Watson, J. G., Kuhns, H., Etyemezian, V., Lowenthal, D. H., Crow, D., Kohl, S. D.,  
881 Engelbrecht, J. P., and Green, M. C.: Source profiles for industrial, mobile, and area sources in  
882 the Big Bend Regional Aerosol Visibility and Observational study, *Chemosphere*, 54, 185-208,  
883 10.1016/j.chemosphere.2003.07.004, 2004.
- 884 Claeys, M., Vermeylen, R., Yasmeen, F., Gómez-González, Y., Chi, X., Maenhaut, W.,  
885 Mészáros, T., and Salma, I.: Chemical characterisation of humic-like substances from urban,  
886 rural and tropical biomass burning environments using liquid chromatography with UV/vis  
887 photodiode array detection and electrospray ionisation mass spectrometry, *Environ Chem*, 9,  
888 273-284, 10.1071/en11163, 2012.
- 889 Cohen, D. D., Stelcer, E., Santos, F. L., Prior, M., Thompson, C., and Pabroa, P. C. B.:  
890 Fingerprinting and source apportionment of fine particle pollution in Manila by IBA and PMF  
891 techniques: A 7-year study, *X-Ray Spectrom*, 38, 18-25, 10.1002/xrs.1112, 2009.
- 892 Crosbie, E., Sorooshian, A., Monfared, N. A., Shingler, T., and Esmaili, O.: A multi-year aerosol  
893 characterization for the greater Tehran area using satellite, surface, and modeling data,  
894 *Atmosphere*, 5, 178-197, 10.3390/atmos5020178, 2014.
- 895 Cruz, F. T., Narisma, G. T., Villafuerte, M. Q., Cheng Chua, K. U., and Olaguera, L. M.: A  
896 climatological analysis of the southwest monsoon rainfall in the Philippines, *Atmos Res*, 122,  
897 609-616, 10.1016/j.atmosres.2012.06.010, 2013.
- 898 Cruz, M. T., Bañaga, P. A., Betito, G., Braun, R. A., Stahl, C., Aghdam, M. A., Cambaliza, M.  
899 O., Dadashazar, H., Hilario, M. R., Lorenzo, G. R., Ma, L., MacDonald, A. B., Pabroa, P. C.,  
900 Yee, J. R., Simpas, J. B., and Sorooshian, A.: Size-resolved composition and morphology of  
901 particulate matter during the southwest monsoon in Metro Manila, Philippines, *Atmos Chem*  
902 *Phys*, 19, 10675-10696, 10.5194/acp-19-10675-2019, 2019.



- 903 Dasgupta, P. K., Campbell, S. W., Al-Horr, R. S., Ullah, S. M. R., Li, J., Amalfitano, C., and  
904 Poor, N. D.: Conversion of sea salt aerosol to NaNO<sub>3</sub> and the production of HCl: Analysis of  
905 temporal behavior of aerosol chloride/nitrate and gaseous HCl/HNO<sub>3</sub> concentrations with AIM,  
906 *Atmos Environ*, 41, 4242-4257, 10.1016/j.atmosenv.2006.09.054, 2007.
- 907 Davis, D., Chen, G., Kasibhatla, P., Jefferson, A., Tanner, D., Eisele, F., Lenschow, D., Neff,  
908 W., and Berresheim, H.: DMS oxidation in the Antarctic marine boundary layer: Comparison of  
909 model simulations and held observations of DMS, DMSO, DMSO<sub>2</sub>, H<sub>2</sub>SO<sub>4</sub>(g), MSA(g), and  
910 MSA(p), *J Geophys Res-Atmos*, 103, 1657-1678, 10.1029/97jd03452, 1998.
- 911 Dawson, M. L., Varner, M. E., Perraud, V., Ezell, M. J., Gerber, R. B., and Finlayson-Pitts, B. J.:  
912 Simplified mechanism for new particle formation from methanesulfonic acid, amines, and water  
913 via experiments and ab initio calculations, *Proc Natl Acad Sci U S A*, 109, 18719-18724,  
914 10.1073/pnas.1211878109, 2012.
- 915 De Bruyn, W. J., Shorter, J. A., Davidovits, P., Worsnop, D. R., Zahniser, M. S., and Kolb, C. E.:  
916 Uptake of gas phase sulfur species methanesulfonic acid, dimethylsulfoxide, and dimethyl  
917 sulfone by aqueous surfaces, *J Geophys Res*, 99, 16927-16932, 10.1029/94jd00684, 1994.
- 918 Decesari, S., Fuzzi, S., Facchini, M. C., Mircea, M., Emblico, L., Cavalli, F., Maenhaut, W., Chi,  
919 X., Schkolnik, G., Falkovich, A., Rudich, Y., Claeys, M., Pashynska, V., Vas, G., Kourtchev, I.,  
920 Vermeylen, R., Hoffer, A., Andreae, M. O., Tagliavini, E., Moretti, F., and Artaxo, P.:  
921 Characterization of the organic composition of aerosols from Rondônia, Brazil, during the LBA-  
922 SMOCC 2002 experiment and its representation through model compounds, *Atmos Chem Phys*,  
923 6, 375-402, 10.5194/acp-6-375-2006, 2006.
- 924 Deshmukh, D. K., Kawamura, K., Lazaar, M., Kunwar, B., and Boreddy, S. K. R.: Dicarboxylic  
925 acids, oxoacids, benzoic acid,  $\alpha$ -dicarbonyls, WSOC, OC, and ions in spring aerosols from  
926 Okinawa Island in the western North Pacific Rim: size distributions and formation processes,  
927 *Atmos Chem Phys*, 16, 5263-5282, 10.5194/acp-16-5263-2016, 2016.
- 928 Dimitriou, K.: The dependence of PM size distribution from meteorology and local-regional  
929 contributions, in Valencia (Spain)-A CWT model approach, *Aerosol Air Qual Res*, 15, 1979-  
930 1989, 10.4209/aaqr.2015.03.0162, 2015.
- 931 Dimitriou, K., Remoundaki, E., Mantas, E., and Kassomenos, P.: Spatial distribution of source  
932 areas of PM<sub>2.5</sub> by Concentration Weighted Trajectory (CWT) model applied in PM<sub>2.5</sub>  
933 concentration and composition data, *Atmos Environ*, 116, 138-145,  
934 10.1016/j.atmosenv.2015.06.021, 2015.
- 935 Ding, X., Wang, X., Xie, Z., Zhang, Z., and Sun, L.: Impacts of Siberian biomass burning on  
936 organic aerosols over the North Pacific Ocean and the Arctic: primary and secondary organic  
937 tracers, *Environ Sci Technol*, 47, 3149-3157, 10.1021/es3037093, 2013.
- 938 Ding, X. X., Kong, L. D., Du, C. T., Zhanzakova, A., Fu, H. B., Tang, X. F., Wang, L., Yang,  
939 X., Chen, J. M., and Cheng, T. T.: Characteristics of size-resolved atmospheric inorganic and  
940 carbonaceous aerosols in urban Shanghai, *Atmos Environ*, 167, 625-641,  
941 10.1016/j.atmosenv.2017.08.043, 2017.
- 942 Drozd, G., Woo, J., Häkkinen, S. A. K., Nenes, A., and McNeill, V. F.: Inorganic salts interact  
943 with oxalic acid in submicron particles to form material with low hygroscopicity and volatility,  
944 *Atmos Chem Phys*, 14, 5205-5215, 10.5194/acp-14-5205-2014, 2014.
- 945 Duarte, R., Matos, J. T. V., Paula, A. S., Lopes, S. P., Pereira, G., Vasconcellos, P., Gioda, A.,  
946 Carreira, R., Silva, A. M. S., Duarte, A. C., Smichowski, P., Rojas, N., and Sanchez-Ccoyllo, O.:  
947 Structural signatures of water-soluble organic aerosols in contrasting environments in South



- 948 America and Western Europe, *Environ Pollut*, 227, 513-525, 10.1016/j.envpol.2017.05.011,  
949 2017.
- 950 Echalar, F., Gaudichet, A., Cachier, H., and Artaxo, P.: Aerosol emissions by tropical forest and  
951 savanna biomass burning: Characteristic trace elements and fluxes, *Geophys Res Lett*, 22, 3039-  
952 3042, 10.1029/95gl03170, 1995.
- 953 Ervens, B., Feingold, G., Clegg, S. L., and Kreidenweis, S. M.: A modeling study of aqueous  
954 production of dicarboxylic acids: 2. Implications for cloud microphysics, *J Geophys Res*, 109,  
955 10.1029/2004jd004575, 2004.
- 956 Ervens, B., Sorooshian, A., Lim, Y. B., and Turpin, B. J.: Key parameters controlling OH-  
957 initiated formation of secondary organic aerosol in the aqueous phase (aqSOA), *J Geophys Res-  
958 Atmos*, 119, 3997-4016, 10.1002/2013jd021021, 2014.
- 959 Ervens, B.: Progress and Problems in Modeling Chemical Processing in Cloud Droplets and Wet  
960 Aerosol Particles, in: *Multiphase Environmental Chemistry in the Atmosphere*, ACS Symposium  
961 Series, ACS Publications, 327-345, 2018.
- 962 Falkovich, A. H., Schkolnik, G., Ganor, E., and Rudich, Y.: Adsorption of organic compounds  
963 pertinent to urban environments onto mineral dust particles, *J Geophys Res*, 109,  
964 10.1029/2003jd003919, 2004.
- 965 Falkovich, A. H., Graber, E. R., Schkolnik, G., Rudich, Y., Maenhaut, W., and Artaxo, P.: Low  
966 molecular weight organic acids in aerosol particles from Rondônia, Brazil, during the biomass-  
967 burning, transition and wet periods, *Atmos Chem Phys*, 5, 781-797, 10.5194/acp-5-781-2005,  
968 2005.
- 969 Fine, P. M., Chakrabarti, B., Krudysz, M., Schauer, J. J., and Sioutas, C.: Diurnal variations of  
970 individual organic compound constituents of ultrafine and accumulation mode particulate matter  
971 in the Los Angeles Basin, *Environ Sci Technol*, 38, 1296-1304, 10.1021/es0348389, 2004.
- 972 Fitzgerald, J. W.: Marine aerosols: A review, *Atmos Environ A-Gen*, 25, 533-545,  
973 10.1016/0960-1686(91)90050-h, 1991.
- 974 Fossum, K. N., Ovadnevaite, J., Ceburnis, D., Dall'Osto, M., Marullo, S., Bellacicco, M., Simo,  
975 R., Liu, D., Flynn, M., Zuend, A., and O'Dowd, C.: Summertime Primary and Secondary  
976 Contributions to Southern Ocean Cloud Condensation Nuclei, *Sci Rep*, 8, 13844,  
977 10.1038/s41598-018-32047-4, 2018.
- 978 Freedman, M. A., Hasenkopf, C. A., Beaver, M. R., and Tolbert, M. A.: Optical properties of  
979 internally mixed aerosol particles composed of dicarboxylic acids and ammonium sulfate, *J Phys  
980 Chem A*, 113, 13584-13592, 10.1021/jp906240y, 2009.
- 981 Fu, P. Q., Kawamura, K., Chen, J., Li, J., Sun, Y. L., Liu, Y., Tachibana, E., Aggarwal, S. G.,  
982 Okuzawa, K., Tanimoto, H., Kanaya, Y., and Wang, Z. F.: Diurnal variations of organic  
983 molecular tracers and stable carbon isotopic composition in atmospheric aerosols over Mt. Tai in  
984 the North China Plain: an influence of biomass burning, *Atmos Chem Phys*, 12, 8359-8375,  
985 10.5194/acp-12-8359-2012, 2012.
- 986 Gao, S., Hegg, D. A., Hobbs, P. V., Kirchstetter, T. W., Magi, B. I., and Sadilek, M.: Water-  
987 soluble organic components in aerosols associated with savanna fires in southern Africa:  
988 Identification, evolution, and distribution, *J Geophys Res-Atmos*, 108, n/a-n/a,  
989 10.1029/2002jd002324, 2003.
- 990 Gao, Y., Arimoto, R., Duce, R. A., Chen, L. Q., Zhou, M. Y., and Gu, D. Y.: Atmospheric non-  
991 sea-salt sulfate, nitrate and methanesulfonate over the China Sea, *J Geophys Res-Atmos*, 101,  
992 12601-12611, 10.1029/96jd00866, 1996.



- 993 Ge, C., Wang, J., Reid, J. S., Posselt, D. J., Xian, P., and Hyer, E.: Mesoscale modeling of smoke  
994 transport from equatorial Southeast Asian Maritime Continent to the Philippines: First  
995 comparison of ensemble analysis with in situ observations, *J Geophys Res-Atmos*, 122, 5380-  
996 5398, 10.1002/2016jd026241, 2017.
- 997 Gelencsér, and Varga: Evaluation of the atmospheric significance of multiphase reactions in  
998 atmospheric secondary organic aerosol formation, *Atmos Chem Phys*, 5, 2823-2831,  
999 10.5194/acp-5-2823-2005, 2005.
- 1000 Golly, B., Waked, A., Weber, S., Samake, A., Jacob, V., Conil, S., Rangognio, J., Chrétien, E.,  
1001 Vagnot, M. P., Robic, P. Y., Besombes, J. L., and Jaffrezo, J. L.: Organic markers and OC source  
1002 apportionment for seasonal variations of PM<sub>2.5</sub> at 5 rural sites in France, *Atmos Environ*, 198,  
1003 142-157, 10.1016/j.atmosenv.2018.10.027, 2019.
- 1004 Gondwe, M., Krol, M., Klaassen, W., Gieskes, W., and de Baar, H.: Comparison of modeled  
1005 versus measured MSA:nss SO<sub>4</sub>=ratios: A global analysis, *Global Biogeochem Cy*, 18, n/a-n/a,  
1006 10.1029/2003gb002144, 2004.
- 1007 Graham, B., Mayol-Bracero, O. L., Guyon, P., Roberts, G. C., Decesari, S., Facchini, M. C.,  
1008 Artaxo, P., Maenhaut, W., Koll, P., and Andreae, M. O.: Water-soluble organic compounds in  
1009 biomass burning aerosols over Amazonia1. Characterization by NMR and GC-MS, *J Geophys*  
1010 *Res*, 107, LBA 14-11-LBA 14-16, 10.1029/2001jd000336, 2002.
- 1011 Greenfield, S. M.: Rain scavenging of radioactive particulate matter from the atmosphere, *J*  
1012 *Meteorol*, 14, 115-125, 10.1175/1520-0469(1957)0142.0.CO;1957.
- 1013 Grosjean, D., Van Cauwenberghe, K., Schmid, J. P., Kelley, P. E., and Pitts, J. N.: Identification  
1014 of C<sub>3</sub>-C<sub>10</sub> aliphatic dicarboxylic acids in airborne particulate matter, *Environ Sci Technol*, 12,  
1015 313-317, 10.1021/es60139a005, 1978.
- 1016 Gullett, B. K., Linak, W. P., Touati, A., Wasson, S. J., Gatica, S., and King, C. J.:  
1017 Characterization of air emissions and residual ash from open burning of electronic wastes during  
1018 simulated rudimentary recycling operations, *J Mater Cycles Waste*, 9, 69-79, 10.1007/s10163-  
1019 006-0161-x, 2007.
- 1020 Hanson, D. R.: Mass accommodation of H<sub>2</sub>SO<sub>4</sub> and CH<sub>3</sub>SO<sub>3</sub>H on water-sulfuric acid solutions  
1021 from 6% to 97% RH, *J Phys Chem A*, 109, 6919-6927, 10.1021/jp0510443, 2005.
- 1022 Harrison, R. M., Beddows, D. C., and Dall'Osto, M.: PMF analysis of wide-range particle size  
1023 spectra collected on a major highway, *Environ Sci Technol*, 45, 5522-5528, 10.1021/es2006622,  
1024 2011.
- 1025 Hatakeyama, S., Ohno, M., Weng, J., Takagi, H., and Akimoto, H.: Mechanism for the formation  
1026 of gaseous and particulate products from ozone-cycloalkene reactions in air, *Environ Sci*  
1027 *Technol*, 21, 52-57, 10.1021/es00155a005, 1987.
- 1028 Hilario, M. R. A., Cruz, M. T., Bañaga, P. A., Betito, G., Braun, R. A., Stahl, C., Cambaliza, M.  
1029 O., Lorenzo, G. R., MacDonald, A. B., AzadiAghdam, M., Pabroa, P. C., Yee, J. R., Simpas, J.  
1030 B., and Sorooshian, A.: Characterizing weekly cycles of particulate matter in a coastal megacity:  
1031 The importance of a seasonal, size-resolved, and chemically-speciated analysis, *J Geophys Res-*  
1032 *Atmos*, Accepted, 10.1029/2020JD032614, 2020a.
- 1033 Hilario, M. R. A., Cruz, M. T., Cambaliza, M. O. L., Reid, J. S., Xian, P., Simpas, J. B.,  
1034 Lagrosas, N. D., Uy, S. N. Y., Cliff, S., and Zhao, Y.: Investigating size-segregated sources of  
1035 elemental composition of particulate matter in the South China Sea during the 2011 Vasco  
1036 cruise, *Atmos Chem Phys*, 20, 1255-1276, 10.5194/acp-20-1255-2020, 2020b.



- 1037 Ho, K. F., Lee, S. C., Cao, J. J., Kawamura, K., Watanabe, T., Cheng, Y., and Chow, J. C.:  
1038 Dicarboxylic acids, ketocarboxylic acids and dicarbonyls in the urban roadside area of Hong  
1039 Kong, *Atmos Environ*, 40, 3030-3040, 10.1016/j.atmosenv.2005.11.069, 2006.
- 1040 Hodshire, A. L., Campuzano-Jost, P., Kodros, J. K., Croft, B., Nault, B. A., Schroder, J. C.,  
1041 Jimenez, J. L., and Pierce, J. R.: The potential role of methanesulfonic acid (MSA) in aerosol  
1042 formation and growth and the associated radiative forcings, *Atmos Chem Phys*, 19, 3137-3160,  
1043 10.5194/acp-19-3137-2019, 2019.
- 1044 Hoffmann, E. H., Tilgner, A., Schrodner, R., Brauer, P., Wolke, R., and Herrmann, H.: An  
1045 advanced modeling study on the impacts and atmospheric implications of multiphase dimethyl  
1046 sulfide chemistry, *Proc Natl Acad Sci U S A*, 113, 11776-11781, 10.1073/pnas.1606320113,  
1047 2016.
- 1048 Hoffmann, E. H., Tilgner, A., Vogelsberg, U., Wolke, R., and Herrmann, H.: Near-Explicit  
1049 Multiphase Modeling of Halogen Chemistry in a Mixed Urban and Maritime Coastal Area, *ACS*  
1050 *Earth and Space Chem*, 3, 2452-2471, 10.1021/acsearthspacechem.9b00184, 2019.
- 1051 Hopke, P. K., Cohen, D. D., Begum, B. A., Biswas, S. K., Ni, B., Pandit, G. G., Santoso, M.,  
1052 Chung, Y.-S., Rahman, S. A., Hamzah, M. S., Davy, P., Markwitz, A., Waheed, S., Siddique, N.,  
1053 Santos, F. L., Pabroa, P. C. B., Seneviratne, M. C. S., Wimolwattanapun, W., Bunprapob, S.,  
1054 Vuong, T. B., and Markowicz, A.: Urban air quality in the Asian region, *Sci Total Environ*, 409,  
1055 4140, 10.1016/j.scitotenv.2011.06.028, 2011.
- 1056 Hsu, S. C., Liu, S. C., Huang, Y. T., Chou, C. C., Lung, S. C., Liu, T. H., Tu, J. Y., and Tsai, F.:  
1057 Long-range southeastward transport of Asian biomass pollution: Signature detected by aerosol  
1058 potassium in northern Taiwan, *J Geophys Res-Atmos*, 114, 10.1029/2009JD011725, 2009.
- 1059 Hsu, Y.-K., Holsen, T. M., and Hopke, P. K.: Comparison of hybrid receptor models to locate  
1060 PCB sources in Chicago, *Atmos Environ*, 37, 545-562, 10.1016/S1352-2310(02)00886-5, 2003.
- 1061 Iijima, A., Sato, K., Yano, K., Tago, H., Kato, M., Kimura, H., and Furuta, N.: Particle size and  
1062 composition distribution analysis of automotive brake abrasion dusts for the evaluation of  
1063 antimony sources of airborne particulate matter, *Atmos Environ*, 41, 4908-4919,  
1064 10.1016/j.atmosenv.2007.02.005, 2007.
- 1065 Jusino-Atresino, R., Anderson, J., and Gao, Y.: Ionic and elemental composition of PM<sub>2.5</sub>  
1066 aerosols over the Caribbean Sea in the Tropical Atlantic, *J Atmos Chem*, 73, 427-457,  
1067 10.1007/s10874-016-9337-5, 2016.
- 1068 Kautzman, K. E., Surratt, J. D., Chan, M. N., Chan, A. W., Hersey, S. P., Chhabra, P. S.,  
1069 Dalleska, N. F., Wennberg, P. O., Flagan, R. C., and Seinfeld, J. H.: Chemical composition of  
1070 gas- and aerosol-phase products from the photooxidation of naphthalene, *J Phys Chem A*, 114,  
1071 913-934, 10.1021/jp908530s, 2010.
- 1072 Kavouras, I. G., and Stephanou, E. G.: Particle size distribution of organic primary and  
1073 secondary aerosol constituents in urban, background marine, and forest atmosphere, *J Geophys*  
1074 *Res*, 107, 10.1029/2000jd000278, 2002.
- 1075 Kawamura, K., Ng, L. L., and Kaplan, I. R.: Determination of organic acids (C<sub>1</sub>-C<sub>10</sub>) in the  
1076 atmosphere, motor exhausts, and engine oils, *Environ Sci Technol*, 19, 1082-1086,  
1077 10.1021/es00141a010, 1985.
- 1078 Kawamura, K., and Kaplan, I. R.: Motor exhaust emissions as a primary source for dicarboxylic  
1079 acids in Los Angeles ambient air, *Environ Sci Technol*, 21, 105-110, 10.1021/es00155a014,  
1080 1987.



- 1081 Kawamura, K., and Sakaguchi, F.: Molecular distributions of water soluble dicarboxylic acids in  
1082 marine aerosols over the Pacific Ocean including tropics, *J Geophys Res-Atmos*, 104, 3501-  
1083 3509, 10.1029/1998jd100041, 1999.
- 1084 Kawamura, K., and Ikushima, K.: Seasonal changes in the distribution of dicarboxylic acids in  
1085 the urban atmosphere, *Environ Sci Technol*, 27, 2227-2235, 10.1021/es00047a033, 2002.
- 1086 Kawamura, K., and Yasui, O.: Diurnal changes in the distribution of dicarboxylic acids,  
1087 ketocarboxylic acids and dicarbonyls in the urban Tokyo atmosphere, *Atmos Environ*, 39, 1945-  
1088 1960, 10.1016/j.atmosenv.2004.12.014, 2005.
- 1089 Kawamura, K., Kasukabe, H., and Barrie, L. A.: Secondary formation of water-soluble organic  
1090 acids and  $\alpha$ -dicarbonyls and their contributions to total carbon and water-soluble organic carbon:  
1091 Photochemical aging of organic aerosols in the Arctic spring, *J Geophys Res*, 115,  
1092 10.1029/2010jd014299, 2010.
- 1093 Kawamura, K., Tachibana, E., Okuzawa, K., Aggarwal, S. G., Kanaya, Y., and Wang, Z. F.:  
1094 High abundances of water-soluble dicarboxylic acids, ketocarboxylic acids and  $\alpha$ -dicarbonyls in  
1095 the mountaintop aerosols over the North China Plain during wheat burning season, *Atmos Chem*  
1096 *Phys*, 13, 8285-8302, 10.5194/acp-13-8285-2013, 2013.
- 1097 Kawamura, K., and Bikkina, S.: A review of dicarboxylic acids and related compounds in  
1098 atmospheric aerosols: Molecular distributions, sources and transformation, *Atmos Res*, 170, 140-  
1099 160, 10.1016/j.atmosres.2015.11.018, 2016.
- 1100 Kecorius, S., Madueño, L., Vallar, E., Alas, H., Betito, G., Birmili, W., Cambaliza, M. O.,  
1101 Catipay, G., Gonzaga-Cayetano, M., Galvez, M. C., Lorenzo, G., Müller, T., Simpas, J. B.,  
1102 Tamayo, E. G., and Wiedensohler, A.: Aerosol particle mixing state, refractory particle number  
1103 size distributions and emission factors in a polluted urban environment: Case study of Metro  
1104 Manila, Philippines, *Atmos Environ*, 170, 169-183, 10.1016/j.atmosenv.2017.09.037, 2017.
- 1105 Kerminen, V.-M., Teinilä, K., Hillamo, R., and Mäkelä, T.: Size-segregated chemistry of  
1106 particulate dicarboxylic acids in the Arctic atmosphere, *Atmos Environ*, 33, 2089-2100,  
1107 10.1016/s1352-2310(98)00350-1, 1999.
- 1108 Kerminen, V.-M., Ojanen, C., Pakkanen, T., Hillamo, R., Aurela, M., and Meriläinen, J.: Low-  
1109 Molecular-Weight Dicarboxylic Acids in an Urban and Rural Atmosphere, *J Aerosol Sci*, 31,  
1110 349-362, 10.1016/s0021-8502(99)00063-4, 2000.
- 1111 Kerminen, V.-M., Aurela, M., Hillamo, R. E., and Virkkula, A.: Formation of particulate MSA:  
1112 deductions from size distribution measurements in the Finnish Arctic, *Tellus B*, 49, 159-171,  
1113 10.3402/tellusb.v49i2.15959, 2017.
- 1114 Kim Oanh, N. T., Upadhyay, N., Zhuang, Y. H., Hao, Z. P., Murthy, D. V. S., Lestari, P.,  
1115 Villarin, J. T., Chengchua, K., Co, H. X., and Dung, N. T.: Particulate air pollution in six Asian  
1116 cities: Spatial and temporal distributions, and associated sources, *Atmos Environ*, 40, 3367-3380,  
1117 10.1016/j.atmosenv.2006.01.050, 2006.
- 1118 Kleindienst, T. E., Jaoui, M., Lewandowski, M., Offenber, J. H., and Docherty, K. S.: The  
1119 formation of SOA and chemical tracer compounds from the photooxidation of naphthalene and  
1120 its methyl analogs in the presence and absence of nitrogen oxides, *Atmos Chem Phys*, 12, 8711-  
1121 8726, 10.5194/acp-12-8711-2012, 2012.
- 1122 Kobayashi, H., Matsunaga, T., Hoyano, A., Aoki, M., Komori, D., and Boonyawat, S.: Satellite  
1123 estimation of photosynthetically active radiation in Southeast Asia: Impacts of smoke and cloud  
1124 cover, *J Geophys Res-Atmos*, 109, n/a-n/a, 10.1029/2003jd003807, 2004.
- 1125 Kondo, Y., Matsui, H., Moteki, N., Sahu, L., Takegawa, N., Kajino, M., Zhao, Y., Cubison, M.  
1126 J., Jimenez, J. L., Vay, S., Diskin, G. S., Anderson, B., Wisthaler, A., Mikoviny, T., Fuelberg, H.



- 1127 E., Blake, D. R., Huey, G., Weinheimer, A. J., Knapp, D. J., and Brune, W. H.: Emissions of  
1128 black carbon, organic, and inorganic aerosols from biomass burning in North America and Asia  
1129 in 2008, *J Geophys Res*, 116, 10.1029/2010jd015152, 2011.
- 1130 Kumar, S., Aggarwal, S. G., Gupta, P. K., and Kawamura, K.: Investigation of the tracers for  
1131 plastic-enriched waste burning aerosols, *Atmos Environ*, 108, 49-58,  
1132 10.1016/j.atmosenv.2015.02.066, 2015.
- 1133 Kundu, S., Kawamura, K., Andreae, T. W., Hoffer, A., and Andreae, M. O.: Molecular  
1134 distributions of dicarboxylic acids, ketocarboxylic acids and  $\alpha$ -dicarbonyls in biomass  
1135 burning aerosols: implications for photochemical production and degradation in smoke layers,  
1136 *Atmos Chem Phys*, 10, 2209-2225, 10.5194/acp-10-2209-2010, 2010.
- 1137 Kunwar, B., Kawamura, K., Fujiwara, S., Fu, P., Miyazaki, Y., and Pokhrel, A.: Dicarboxylic  
1138 acids, oxocarboxylic acids and  $\alpha$ -dicarbonyls in atmospheric aerosols from Mt. Fuji, Japan:  
1139 Implication for primary emission versus secondary formation, *Atmos Res*, 221, 58-71,  
1140 10.1016/j.atmosres.2019.01.021, 2019.
- 1141 Li, J., Wang, G., Zhang, Q., Li, J., Wu, C., Jiang, W., Zhu, T., and Zeng, L.: Molecular  
1142 characteristics and diurnal variations of organic aerosols at a rural site in the North China Plain  
1143 with implications for the influence of regional biomass burning, *Atmos Chem Phys*, 19, 10481-  
1144 10496, 10.5194/acp-19-10481-2019, 2019.
- 1145 Limbeck, A., Puxbaum, H., Otter, L., and Scholes, M. C.: Semivolatile behavior of dicarboxylic  
1146 acids and other polar organic species at a rural background site (Nylsvley, RSA), *Atmos*  
1147 *Environ*, 35, 1853-1862, 10.1016/s1352-2310(00)00497-0, 2001.
- 1148 Linak, W. P., Miller, C. A., and Wendt, J. O.: Comparison of particle size distributions and  
1149 elemental partitioning from the combustion of pulverized coal and residual fuel oil, *J Air Waste*  
1150 *Manag Assoc*, 50, 1532-1544, 10.1080/10473289.2000.10464171, 2000.
- 1151 Liu, Y., Minofar, B., Desyaterik, Y., Dames, E., Zhu, Z., Cain, J. P., Hopkins, R. J., Gilles, M.  
1152 K., Wang, H., Jungwirth, P., and Laskin, A.: Internal structure, hygroscopic and reactive  
1153 properties of mixed sodium methanesulfonate-sodium chloride particles, *Phys Chem Chem Phys*,  
1154 13, 11846-11857, 10.1039/c1cp20444k, 2011.
- 1155 Ma, L., Dadashazar, H., Braun, R. A., MacDonald, A. B., Aghdam, M. A., Maudlin, L. C., and  
1156 Sorooshian, A.: Size-resolved characteristics of water-soluble particulate elements in a coastal  
1157 area: Source identification, influence of wildfires, and diurnal variability, *Atmos Environ*, 206,  
1158 72-84, 10.1016/j.atmosenv.2019.02.045, 2019.
- 1159 Madueño, L., Kecorius, S., Birmili, W., Müller, T., Simpas, J., Vallar, E., Galvez, M. C.,  
1160 Cayetano, M., and Wiedensohler, A.: Aerosol Particle and Black Carbon Emission Factors of  
1161 Vehicular Fleet in Manila, Philippines, *Atmosphere*, 10, 603, 10.3390/atmos10100603, 2019.
- 1162 Maenhaut, W., Wang, W., and Chi, X.: Semivolatile behaviour and filter sampling artifacts for  
1163 dicarboxylic acids during summer campaigns at three forested sites in Europe, *Boreal Environ*  
1164 *Res*, 16, 273-287, 2011.
- 1165 Mahowald, N., Jickells, T. D., Baker, A. R., Artaxo, P., Benitez-Nelson, C. R., Bergametti, G.,  
1166 Bond, T. C., Chen, Y., Cohen, D. D., Herut, B., Kubilay, N., Losno, R., Luo, C., Maenhaut, W.,  
1167 McGee, K. A., Okin, G. S., Siefert, R. L., and Tsukuda, S.: Global distribution of atmospheric  
1168 phosphorus sources, concentrations and deposition rates, and anthropogenic impacts, *Global*  
1169 *Biogeochem Cy*, 22, n/a-n/a, 10.1029/2008gb003240, 2008.
- 1170 Malm, W. C., Sisler, J. F., Huffman, D., Eldred, R. A., and Cahill, T. A.: Spatial and seasonal  
1171 trends in particle concentration and optical extinction in the United States, *J Geophys Res-*  
1172 *Atmos*, 99, 1347-1370, 10.1029/93jd02916, 1994.



- 1173 Mardi, A. H., Dadashazar, H., MacDonald, A. B., Braun, R. A., Crosbie, E., Xian, P., Thorsen,  
1174 T. J., Coggon, M. M., Fenn, M. A., Ferrare, R. A., Hair, J. W., Woods, R. K., Jonsson, H. H.,  
1175 Flagan, R. C., Seinfeld, J. H., and Sorooshian, A.: Biomass Burning Plumes in the Vicinity of the  
1176 California Coast: Airborne Characterization of Physicochemical Properties, Heating Rates, and  
1177 Spatiotemporal Features, *J Geophys Res-Atmos*, 123, 13,560-513,582, 10.1029/2018jd029134,  
1178 2018.
- 1179 Marple, V., Olson, B., Romay, F., Hudak, G., Geerts, S. M., and Lundgren, D.: Second  
1180 Generation Micro-Orifice Uniform Deposit Impactor, 120 MOUDI-II: Design, Evaluation, and  
1181 Application to Long-Term Ambient Sampling, *Aerosol Sci. Tech.*, 48, 427-433,  
1182 10.1080/02786826.2014.884274, 2014.
- 1183 Marsh, A., Miles, R. E. H., Rovelli, G., Cowling, A. G., Nandy, L., Dutcher, C. S., and Reid, J.  
1184 P.: Influence of organic compound functionality on aerosol hygroscopicity: dicarboxylic acids,  
1185 alkyl-substituents, sugars and amino acids, *Atmos Chem Phys*, 17, 5583-5599, 10.5194/acp-17-  
1186 5583-2017, 2017.
- 1187 Marsh, A., Rovelli, G., Miles, R. E. H., and Reid, J. P.: Complexity of Measuring and  
1188 Representing the Hygroscopicity of Mixed Component Aerosol, *J Phys Chem A*, 123, 1648-  
1189 1660, 10.1021/acs.jpca.8b11623, 2019.
- 1190 Matsumoto, J., Olaguera, L. M. P., Nguyen-Le, D., Kubota, H., and Villafuerte, M. Q.:  
1191 Climatological seasonal changes of wind and rainfall in the Philippines, *Int J Climatol*,  
1192 10.1002/joc.6492, 2020.
- 1193 Maudlin, L. C., Wang, Z., Jonsson, H. H., and Sorooshian, A.: Impact of wildfires on size-  
1194 resolved aerosol composition at a coastal California site, *Atmos Environ*, 119, 59-68,  
1195 10.1016/j.atmosenv.2015.08.039, 2015.
- 1196 McGinty, S. M., Kapala, M. K., and Niedziela, R. F.: Mid-infrared complex refractive indices for  
1197 oleic acid and optical properties of model oleic acid/water aerosols, *Phys Chem Chem Phys*, 11,  
1198 7998-8004, 10.1039/b905371a, 2009.
- 1199 Mochida, M., Umemoto, N., Kawamura, K., and Uematsu, M.: Bimodal size distribution of C2-  
1200 C4dicarboxylic acids in the marine aerosols, *Geophys Res Lett*, 30, 10.1029/2003gl017451,  
1201 2003.
- 1202 Mooibroek, D., Schaap, M., Weijers, E. P., and Hoogerbrugge, R.: Source apportionment and  
1203 spatial variability of PM<sub>2.5</sub> using measurements at five sites in the Netherlands, *Atmos Environ*,  
1204 45, 4180-4191, 10.1016/j.atmosenv.2011.05.017, 2011.
- 1205 Mora, M., Braun, R. A., Shingler, T., and Sorooshian, A.: Analysis of remotely sensed and  
1206 surface data of aerosols and meteorology for the Mexico Megalopolis Area between 2003 and  
1207 2015, *J Geophys Res Atmos*, 122, 8705-8723, 10.1002/2017JD026739, 2017.
- 1208 Myhre, C. E. L., and Nielsen, C. J.: Optical properties in the UV and visible spectral region of  
1209 organic acids relevant to tropospheric aerosols, *Atmos Chem Phys*, 4, 1759-1769, 10.5194/acp-4-  
1210 1759-2004, 2004.
- 1211 Narukawa, M., Kawamura, K., Takeuchi, N., and Nakajima, T.: Distribution of dicarboxylic  
1212 acids and carbon isotopic compositions in aerosols from 1997 Indonesian forest fires, *Geophys*  
1213 *Res Lett*, 26, 3101-3104, 10.1029/1999gl010810, 1999.
- 1214 Neusüss, C., Pelzing, M., Plewka, A., and Herrmann, H.: A new analytical approach for size-  
1215 resolved speciation of organic compounds in atmospheric aerosol particles: Methods and first  
1216 results, *J Geophys Res-Atmos*, 105, 4513-4527, 10.1029/1999jd901038, 2000.
- 1217 Nguyen, D. L., Kawamura, K., Ono, K., Ram, S. S., Engling, G., Lee, C.-T., Lin, N.-H., Chang,  
1218 S.-C., Chuang, M.-T., and Hsiao, T.-C.: Comprehensive PM<sub>2.5</sub> organic molecular composition



- 1219 and stable carbon isotope ratios at Sonla, Vietnam: Fingerprint of biomass burning components,  
1220 *Aerosol Air Qual Res*, 16, 2618-2634, 10.4209/aaqr.2015.07.0459 2016.
- 1221 Norton, R. B., Roberts, J. M., and Huebert, B. J.: Tropospheric oxalate, *Geophys Res Lett*, 10,  
1222 517-520, 10.1029/GL010i007p00517, 1983.
- 1223 Ovadnevaite, J., Ceburnis, D., Leinert, S., Dall'Osto, M., Canagaratna, M., O'Doherty, S.,  
1224 Berresheim, H., and O'Dowd, C.: Submicron NE Atlantic marine aerosol chemical composition  
1225 and abundance: Seasonal trends and air mass categorization, *J Geophys Res-Atmos*, 119, 11,850-  
1226 811,863, 10.1002/2013jd021330, 2014.
- 1227 Pabroa, P. C. B., Santos, F. L., Morco, R. P., Racho, J. M. D., Bautista Vii, A. T., and Bucal, C.  
1228 G. D.: Receptor modeling studies for the characterization of air particulate lead pollution sources  
1229 in Valenzuela sampling site (Philippines), *Atmos Pollut Res*, 2, 213-218, 10.5094/apr.2011.027,  
1230 2011.
- 1231 PAGASA: Onset of the rainy season: <http://bagong.pagasa.dost.gov.ph/press-release/29#>, 2018a.  
1232 PAGASA: Onset of the northeast monsoon: <http://bagong.pagasa.dost.gov.ph/press-release/32>,  
1233 2018b.
- 1234 PAGASA: Termination of the southwest monsoon: [http://bagong.pagasa.dost.gov.ph/press-](http://bagong.pagasa.dost.gov.ph/press-release/30)  
1235 [release/30](http://bagong.pagasa.dost.gov.ph/press-release/30), 2018c.
- 1236 PAGASA: Transition to northeast monsoon: <http://bagong.pagasa.dost.gov.ph/press-release/56>,  
1237 2019a.
- 1238 PAGASA: Onset of the rainy season: <http://bagong.pagasa.dost.gov.ph/press-release/50>, 2019b.
- 1239 Peng, C., and Chan, C. K.: The water cycles of water-soluble organic salts of atmospheric  
1240 importance, *Atmos Environ*, 35, 1183-1192, 10.1016/s1352-2310(00)00426-x, 2001.
- 1241 Peng, C., Jing, B., Guo, Y. C., Zhang, Y. H., and Ge, M. F.: Hygroscopic Behavior of  
1242 Multicomponent Aerosols Involving NaCl and Dicarboxylic Acids, *J Phys Chem A*, 120, 1029-  
1243 1038, 10.1021/acs.jpca.5b09373, 2016.
- 1244 Pereira, W. E., Rostad, C. E., Taylor, H. E., and Klein, J. M.: Characterization of organic  
1245 contaminants in environmental samples associated with Mount St. Helens 1980 volcanic  
1246 eruption, *Environ Sci Technol*, 16, 387-396, 10.1021/es00101a005, 1982.
- 1247 Prabhakar, G., Sorooshian, A., Toffol, E., Arellano, A. F., and Betterton, E. A.: Spatiotemporal  
1248 Distribution of Airborne Particulate Metals and Metalloids in a Populated Arid Region, *Atmos*  
1249 *Environ*, 92, 339-347, 10.1016/j.atmosenv.2014.04.044, 2014.
- 1250 Pratt, K. A., Murphy, S. M., Subramanian, R., DeMott, P. J., Kok, G. L., Campos, T., Rogers, D.  
1251 C., Prenni, A. J., Heymsfield, A. J., Seinfeld, J. H., and Prather, K. A.: Flight-based chemical  
1252 characterization of biomass burning aerosols within two prescribed burn smoke plumes, *Atmos*  
1253 *Chem Phys*, 11, 12549-12565, 10.5194/acp-11-12549-2011, 2011.
- 1254 Prenni, A. J., DeMott, P. J., Kreidenweis, S. M., Sherman, D. E., Russell, L. M., and Ming, Y.:  
1255 The Effects of Low Molecular Weight Dicarboxylic Acids on Cloud Formation, *J Phys Chem A*,  
1256 105, 11240-11248, 10.1021/jp012427d, 2001.
- 1257 PSA: Highlights of the Philippine population 2015 census of population:  
1258 <https://psa.gov.ph/content/highlights-philippine-population-2015-census-population>, access:  
1259 January 7, 2016.
- 1260 Ramachandran, S., and Rajesh, T. A.: Black carbon aerosol mass concentrations over  
1261 Ahmedabad, an urban location in western India: Comparison with urban sites in Asia, Europe,  
1262 Canada, and the United States, *J Geophys Res*, 112, 10.1029/2006jd007488, 2007.



- 1263 Ran, L., Deng, Z. Z., Wang, P. C., and Xia, X. A.: Black carbon and wavelength-dependent  
1264 aerosol absorption in the North China Plain based on two-year aethalometer measurements,  
1265 *Atmos Environ*, 142, 132-144, 10.1016/j.atmosenv.2016.07.014, 2016.
- 1266 Reff, A., Eberly, S. I., and Bhawe, P. V.: Receptor modeling of ambient particulate matter data  
1267 using positive matrix factorization: review of existing methods, *J Air Waste Manag Assoc*, 57,  
1268 146-154, 10.1080/10473289.2007.10465319, 2007.
- 1269 Reid, J. S., Hobbs, P. V., Ferek, R. J., Blake, D. R., Martins, J. V., Dunlap, M. R., and Liousse,  
1270 C.: Physical, chemical, and optical properties of regional hazes dominated by smoke in Brazil, *J*  
1271 *Geophys Res-Atmos*, 103, 32059-32080, 10.1029/98jd00458, 1998.
- 1272 Reid, J. S., Koppmann, R., Eck, T. F., and Eleuterio, D. P.: A review of biomass burning  
1273 emissions part II: intensive physical properties of biomass burning particles, *Atmos Chem Phys*,  
1274 5, 799-825, 10.5194/acp-5-799-2005, 2005.
- 1275 Reid, J. S., Hyer, E. J., Johnson, R. S., Holben, B. N., Yokelson, R. J., Zhang, J., Campbell, J. R.,  
1276 Christopher, S. A., Di Girolamo, L., Giglio, L., Holz, R. E., Kearney, C., Miettinen, J., Reid, E.  
1277 A., Turk, F. J., Wang, J., Xian, P., Zhao, G., Balasubramanian, R., Chew, B. N., Janjai, S.,  
1278 Lagrosas, N., Lestari, P., Lin, N.-H., Mahmud, M., Nguyen, A. X., Norris, B., Oanh, N. T. K.,  
1279 Oo, M., Salinas, S. V., Welton, E. J., and Liew, S. C.: Observing and understanding the  
1280 Southeast Asian aerosol system by remote sensing: An initial review and analysis for the Seven  
1281 Southeast Asian Studies (7SEAS) program, *Atmos Res*, 122, 403-468,  
1282 10.1016/j.atmosres.2012.06.005, 2013.
- 1283 Reid, J. S., Xian, P., Holben, B. N., Hyer, E. J., Reid, E. A., Salinas, S. V., Zhang, J., Campbell,  
1284 J. R., Chew, B. N., Holz, R. E., Kuciauskas, A. P., Lagrosas, N., Posselt, D. J., Sampson, C. R.,  
1285 Walker, A. L., Welton, E. J., and Zhang, C.: Aerosol meteorology of the Maritime Continent for  
1286 the 2012 7SEAS southwest monsoon intensive study – Part 1: regional-scale phenomena, *Atmos*  
1287 *Chem Phys*, 16, 14041-14056, 10.5194/acp-16-14041-2016, 2016.
- 1288 Rogge, W. F., Mazurek, M. A., Hildemann, L. M., Cass, G. R., and Simoneit, B. R. T.:  
1289 Quantification of urban organic aerosols at a molecular level: Identification, abundance and  
1290 seasonal variation, *Atmos Environ A-Gen*, 27, 1309-1330, 10.1016/0960-1686(93)90257-y,  
1291 1993.
- 1292 Rolph, G., Stein, A., and Stunder, B.: Real-time Environmental Applications and Display  
1293 sYstem: READY, *Environ Modell Softw*, 95, 210-228, 10.1016/j.envsoft.2017.06.025, 2017.
- 1294 Rose, C., Chaumerliac, N., Deguillaume, L., Perroux, H., Mouchel-Vallon, C., Leriche, M.,  
1295 Patryl, L., and Armand, P.: Modeling the partitioning of organic chemical species in cloud  
1296 phases with CLEPS (1.1), *Atmos Chem Phys*, 18, 2225-2242, 10.5194/acp-18-2225-2018, 2018.
- 1297 Russell, L. M., Maria, S. F., and Myneni, S. C. B.: Mapping organic coatings on atmospheric  
1298 particles, *Geophys Res Lett*, 29, 26-21-26-24, 10.1029/2002gl014874, 2002.
- 1299 Saltzman, E. S., Savoie, D. L., Zika, R. G., and Prospero, J. M.: Methane sulfonic acid in the  
1300 marine atmosphere, *J Geophys Res-Oceans*, 88, 10897-10902, 10.1029/JC088iC15p10897, 1983.
- 1301 Sareen, N., Carlton, A. G., Surratt, J. D., Gold, A., Lee, B., Lopez-Hilfiker, F. D., Mohr, C.,  
1302 Thornton, J. A., Zhang, Z., Lim, Y. B., and Turpin, B. J.: Identifying precursors and aqueous  
1303 organic aerosol formation pathways during the SOAS campaign, *Atmos Chem Phys*, 16, 14409-  
1304 14420, 10.5194/acp-16-14409-2016, 2016.
- 1305 Saxena, P., and Hildemann, L. M.: Water-soluble organics in atmospheric particles: A critical  
1306 review of the literature and application of thermodynamics to identify candidate compounds, *J*  
1307 *Atmos Chem*, 24, 57-109, 10.1007/bf00053823, 1996.



- 1308 Schlosser, J. S., Braun, R. A., Bradley, T., Dadashazar, H., MacDonald, A. B., Aldhaif, A. A.,  
1309 Aghdam, M. A., Mardi, A. H., Xian, P., and Sorooshian, A.: Analysis of aerosol composition  
1310 data for western United States wildfires between 2005 and 2015: Dust emissions, chloride  
1311 depletion, and most enhanced aerosol constituents, *J Geophys Res-Atmos*, 122, 8951-8966,  
1312 2017.
- 1313 Seinfeld, J. H., and Pandis, S. N.: *Atmospheric chemistry and physics*, 3rd ed., Wiley-  
1314 Interscience, New York, 2016.
- 1315 Sempère, R., and Kawamura, K.: Comparative distributions of dicarboxylic acids and related  
1316 polar compounds in snow, rain and aerosols from urban atmosphere, *Atmos Environ*, 28, 449-  
1317 459, 10.1016/1352-2310(94)90123-6, 1994.
- 1318 Simoneit, B. R., Medeiros, P. M., and Didyk, B. M.: Combustion products of plastics as  
1319 indicators for refuse burning in the atmosphere, *Environ Sci Technol*, 39, 6961-6970,  
1320 10.1021/es050767x, 2005.
- 1321 Simpas, J., Lorenzo, G., and Cruz, M.: Monitoring Particulate Matter Levels and Composition  
1322 for Source Apportionment Study in Metro Manila, Philippines, in: *Improving Air Quality in  
1323 Asian Developing Countries: Compilation of Research Findings*, edited by: Kim Oanh, N. T.,  
1324 239-261, 2014.
- 1325 Singh, M., Jaques, P. A., and Sioutas, C.: Size distribution and diurnal characteristics of particle-  
1326 bound metals in source and receptor sites of the Los Angeles Basin, *Atmos Environ*, 36, 1675-  
1327 1689, 10.1016/s1352-2310(02)00166-8, 2002.
- 1328 Skyllakou, K., Fountoukis, C., Charalampidis, P., and Pandis, S. N.: Volatility-resolved source  
1329 apportionment of primary and secondary organic aerosol over Europe, *Atmos Environ*, 167, 1-  
1330 10, 10.1016/j.atmosenv.2017.08.005, 2017.
- 1331 Song, J., Zhao, Y., Zhang, Y., Fu, P., Zheng, L., Yuan, Q., Wang, S., Huang, X., Xu, W., Cao,  
1332 Z., Gromov, S., and Lai, S.: Influence of biomass burning on atmospheric aerosols over the  
1333 western South China Sea: Insights from ions, carbonaceous fractions and stable carbon isotope  
1334 ratios, *Environ Pollut*, 242, 1800-1809, 10.1016/j.envpol.2018.07.088, 2018.
- 1335 Sorooshian, A., Varutbangkul, V., Brechtel, F. J., Ervens, B., Feingold, G., Bahreini, R.,  
1336 Murphy, S. M., Holloway, J. S., Atlas, E. L., Buzorius, G., Jonsson, H., Flagan, R. C., and  
1337 Seinfeld, J. H.: Oxalic acid in clear and cloudy atmospheres: Analysis of data from International  
1338 Consortium for Atmospheric Research on Transport and Transformation 2004, *J Geophys Res-  
1339 Atmos*, 111, 10.1029/2005jd006880, 2006.
- 1340 Sorooshian, A., Lu, M. L., Brechtel, F. J., Jonsson, H., Feingold, G., Flagan, R. C., and Seinfeld,  
1341 J. H.: On the source of organic acid aerosol layers above clouds, *Environ Sci Technol*, 41, 4647-  
1342 4654, 10.1021/es0630442, 2007a.
- 1343 Sorooshian, A., Ng, N. L., Chan, A. W. H., Feingold, G., Flagan, R. C., and Seinfeld, J. H.:  
1344 Particulate organic acids and overall water-soluble aerosol composition measurements from the  
1345 2006 Gulf of Mexico Atmospheric Composition and Climate Study (GoMACCS), *J Geophys  
1346 Res-Atmos*, 112, n/a-n/a, 10.1029/2007jd008537, 2007b.
- 1347 Sorooshian, A., Hersey, S., Brechtel, F. J., Corless, A., Flagan, R. C., and Seinfeld, J. H.: Rapid,  
1348 Size-Resolved Aerosol Hygroscopic Growth Measurements: Differential Aerosol Sizing and  
1349 Hygroscopicity Spectrometer Probe (DASH-SP), *Aerosol Sci. Tech.*, 42, 445-464,  
1350 10.1080/02786820802178506, 2008.
- 1351 Sorooshian, A., Padró, L. T., Nenes, A., Feingold, G., McComiskey, A., Hersey, S. P., Gates, H.,  
1352 Jonsson, H. H., Miller, S. D., Stephens, G. L., Flagan, R. C., and Seinfeld, J. H.: On the link  
1353 between ocean biota emissions, aerosol, and maritime clouds: Airborne, ground, and satellite



- 1354 measurements off the coast of California, *Global Biogeochem Cy*, 23, n/a-n/a,  
1355 10.1029/2009gb003464, 2009.
- 1356 Sorooshian, A., Murphy, S. M., Hersey, S., Bahreini, R., Jonsson, H., Flagan, R. C., and  
1357 Seinfeld, J. H.: Constraining the contribution of organic acids and AMSm/z44 to the organic  
1358 aerosol budget: On the importance of meteorology, aerosol hygroscopicity, and region, *Geophys*  
1359 *Res Lett*, 37, n/a-n/a, 10.1029/2010gl044951, 2010.
- 1360 Sorooshian, A., Wonaschutz, A., Jarjour, E. G., Hashimoto, B. I., Schichtel, B. A., and Betterton,  
1361 E. A.: An aerosol climatology for a rapidly growing arid region (southern Arizona): Major  
1362 aerosol species and remotely sensed aerosol properties, *J Geophys Res Atmos*, 116, 16,  
1363 10.1029/2011JD016197, 2011.
- 1364 Sorooshian, A., Crosbie, E., Maudlin, L. C., Youn, J. S., Wang, Z., Shingler, T., Ortega, A. M.,  
1365 Hersey, S., and Woods, R. K.: Surface and Airborne Measurements of Organosulfur and  
1366 Methanesulfonate Over the Western United States and Coastal Areas, *J Geophys Res Atmos*,  
1367 120, 8535-8548, 10.1002/2015JD023822, 2015.
- 1368 Souza, S. R., Vasconcellos, P., and Carvalho, L. R.: Low molecular weight carboxylic acids in  
1369 an urban atmosphere: Winter measurements in Sao Paulo City, Brazil, *Atmos Environ*, 33, 2563-  
1370 2574, 10.1016/s1352-2310(98)00383-5, 1999.
- 1371 Stahl, C., Cruz, M. T., Banaga, P. A., Betito, G., Braun, R. A., Aghdam, M. A., Cambaliza, M.  
1372 O., Lorenzo, G. R., MacDonald, A. B., Pabroa, P. C., Yee, J. R., Simpas, J. B., and Sorooshian,  
1373 A.: An annual time series of weekly size-resolved aerosol properties in the megacity of Metro  
1374 Manila, Philippines, figshare, <https://doi.org/10.6084/m9.figshare.11861859>, 2020a
- 1375 Stahl, C., Cruz, M. T., Banaga, P. A., Betito, G., Braun, R. A., Aghdam, M. A., Cambaliza, M.  
1376 O., Lorenzo, G. R., MacDonald, A. B., Pabroa, P. C., Yee, J. R., Simpas, J. B., and Sorooshian,  
1377 A.: An annual time series of weekly size-resolved aerosol properties in the megacity of Metro  
1378 Manila, Philippines, *Sci Data*, 7, 128, 10.1038/s41597-020-0466-y, 2020b.
- 1379 Stein, A. F., Draxler, R. R., Rolph, G. D., Stunder, B. J. B., Cohen, M. D., and Ngan, F.:  
1380 NOAA's HYSPLIT Atmospheric Transport and Dispersion Modeling System, *B Am Meteorol*  
1381 *Soc*, 96, 2059-2077, 10.1175/bams-d-14-00110.1, 2015.
- 1382 Streets, D. G., Carmichael, G. R., and Arndt, R. L.: Sulfur dioxide emissions and sulfur  
1383 deposition from international shipping in Asian waters, *Atmos Environ*, 31, 1573-1582,  
1384 10.1016/s1352-2310(96)00204-x, 1997.
- 1385 Streets, D. G., Guttikunda, S. K., and Carmichael, G. R.: The growing contribution of sulfur  
1386 emissions from ships in Asian waters, 1988-1995, *Atmos Environ*, 34, 4425-4439,  
1387 10.1016/s1352-2310(00)00175-8, 2000.
- 1388 Sullivan, R. C., and Prather, K. A.: Investigations of the diurnal cycle and mixing state of oxalic  
1389 acid in individual particles in Asian aerosol outflow, *Environ Sci Technol*, 41, 8062-8069,  
1390 10.1021/es071134g, 2007.
- 1391 Sun, Y., Wang, Z., Dong, H., Yang, T., Li, J., Pan, X., Chen, P., and Jayne, J. T.:  
1392 Characterization of summer organic and inorganic aerosols in Beijing, China with an Aerosol  
1393 Chemical Speciation Monitor, *Atmos Environ*, 51, 250-259, 10.1016/j.atmosenv.2012.01.013,  
1394 2012.
- 1395 Takahashi, K., Nansai, K., Tohno, S., Nishizawa, M., Kurokawa, J.-i., and Ohara, T.:  
1396 Production-based emissions, consumption-based emissions and consumption-based health  
1397 impacts of PM<sub>2.5</sub> carbonaceous aerosols in Asia, *Atmos Environ*, 97, 406-415,  
1398 10.1016/j.atmosenv.2014.04.028, 2014.



- 1399 Tang, M., Guo, L., Bai, Y., Huang, R.-J., Wu, Z., Wang, Z., Zhang, G., Ding, X., Hu, M., and  
1400 Wang, X.: Impacts of methanesulfonate on the cloud condensation nucleation activity of sea salt  
1401 aerosol, *Atmos Environ*, 201, 13-17, 10.1016/j.atmosenv.2018.12.034, 2019.
- 1402 Tang, M. J., Whitehead, J., Davidson, N. M., Pope, F. D., Alfarra, M. R., McFiggans, G., and  
1403 Kalberer, M.: Cloud condensation nucleation activities of calcium carbonate and its atmospheric  
1404 ageing products, *Phys Chem Chem Phys*, 17, 32194-32203, 10.1039/c5cp03795f, 2015.
- 1405 Thepnuan, D., Chantara, S., Lee, C. T., Lin, N. H., and Tsai, Y. I.: Molecular markers for  
1406 biomass burning associated with the characterization of PM<sub>2.5</sub> and component sources during  
1407 dry season haze episodes in Upper South East Asia, *Sci Total Environ*, 658, 708-722,  
1408 10.1016/j.scitotenv.2018.12.201, 2019.
- 1409 Tsai, Y. I., Kuo, S.-C., Young, L.-H., Hsieh, L.-Y., and Chen, P.-T.: Atmospheric dry plus wet  
1410 deposition and wet-only deposition of dicarboxylic acids and inorganic compounds in a coastal  
1411 suburban environment, *Atmos Environ*, 89, 696-706, 10.1016/j.atmosenv.2014.03.013, 2014.
- 1412 van Drooge, B. L., and Grimalt, J. O.: Particle size-resolved source apportionment of primary  
1413 and secondary organic tracer compounds at urban and rural locations in Spain, *Atmos Chem  
1414 Phys*, 15, 7735-7752, 10.5194/acp-15-7735-2015, 2015.
- 1415 van Pinxteren, M., Fiedler, B., van Pinxteren, D., Iinuma, Y., Körtzinger, A., and Herrmann, H.:  
1416 Chemical characterization of sub-micrometer aerosol particles in the tropical Atlantic Ocean:  
1417 marine and biomass burning influences, *J Atmos Chem*, 72, 105-125, 10.1007/s10874-015-9307-  
1418 3, 2015.
- 1419 Vasconcellos, P. C., Souza, D. Z., Sanchez-Ccoyllo, O., Bustillos, J. O., Lee, H., Santos, F. C.,  
1420 Nascimento, K. H., Araujo, M. P., Saarnio, K., Teinila, K., and Hillamo, R.: Determination of  
1421 anthropogenic and biogenic compounds on atmospheric aerosol collected in urban, biomass  
1422 burning and forest areas in Sao Paulo, Brazil, *Sci Total Environ*, 408, 5836-5844,  
1423 10.1016/j.scitotenv.2010.08.012, 2010.
- 1424 Virkkula, A., Teinilä, K., Hillamo, R., Kerminen, V. M., Saarikoski, S., Aurela, M., Viidanoja,  
1425 J., Paatero, J., Koponen, I. K., and Kulmala, M.: Chemical composition of boundary layer  
1426 aerosol over the Atlantic Ocean and at an Antarctic site, *Atmos Chem Phys*, 6, 3407-3421,  
1427 10.5194/acp-6-3407-2006, 2006.
- 1428 Wang, G., Xie, M., Hu, S., Gao, S., Tachibana, E., and Kawamura, K.: Dicarboxylic acids,  
1429 metals and isotopic compositions of C and N in atmospheric aerosols from inland China:  
1430 implications for dust and coal burning emission and secondary aerosol formation, *Atmos Chem  
1431 Phys*, 10, 6087-6096, 10.5194/acp-10-6087-2010, 2010.
- 1432 Wang, G., Chen, C., Li, J., Zhou, B., Xie, M., Hu, S., Kawamura, K., and Chen, Y.: Molecular  
1433 composition and size distribution of sugars, sugar-alcohols and carboxylic acids in airborne  
1434 particles during a severe urban haze event caused by wheat straw burning, *Atmos Environ*, 45,  
1435 2473-2479, 10.1016/j.atmosenv.2011.02.045, 2011.
- 1436 Wang, G., Kawamura, K., Cheng, C., Li, J., Cao, J., Zhang, R., Zhang, T., Liu, S., and Zhao, Z.:  
1437 Molecular distribution and stable carbon isotopic composition of dicarboxylic acids,  
1438 ketocarboxylic acids, and alpha-dicarbonyls in size-resolved atmospheric particles from Xi'an  
1439 City, China, *Environ Sci Technol*, 46, 4783-4791, 10.1021/es204322c, 2012.
- 1440 Wang, G., Kawamura, K., Xie, M., Hu, S., Li, J., Zhou, B., Cao, J., and An, Z.: Selected water-  
1441 soluble organic compounds found in size-resolved aerosols collected from urban, mountain and  
1442 marine atmospheres over East Asia, *Tellus B*, 63, 371-381, 10.1111/j.1600-0889.2011.00536.x,  
1443 2017.



- 1444 Wang, J., Ge, C., Yang, Z., Hyer, E. J., Reid, J. S., Chew, B.-N., Mahmud, M., Zhang, Y., and  
1445 Zhang, M.: Mesoscale modeling of smoke transport over the Southeast Asian Maritime  
1446 Continent: Interplay of sea breeze, trade wind, typhoon, and topography, *Atmos Res*, 122, 486-  
1447 503, 10.1016/j.atmosres.2012.05.009, 2013.
- 1448 Wang, Y. Q., Zhang, X. Y., and Draxler, R. R.: TrajStat: GIS-based software that uses various  
1449 trajectory statistical analysis methods to identify potential sources from long-term air pollution  
1450 measurement data, *Environ Modell Softw*, 24, 938-939, 10.1016/j.envsoft.2009.01.004, 2009.
- 1451 Warneck, P.: Multi-Phase Chemistry of C2 and C3 Organic Compounds in the Marine  
1452 Atmosphere, *J Atmos Chem*, 51, 119-159, 10.1007/s10874-005-5984-7, 2005.
- 1453 Wasson, S. J., Linak, W. P., Gullett, B. K., King, C. J., Touati, A., Huggins, F. E., Chen, Y.,  
1454 Shah, N., and Huffman, G. P.: Emissions of chromium, copper, arsenic, and PCDDs/Fs from  
1455 open burning of CCA-treated wood, *Environ Sci Technol*, 39, 8865-8876, 10.1021/es050891g,  
1456 2005.
- 1457 Wonaschuetz, A., Sorooshian, A., Ervens, B., Chuang, P. Y., Feingold, G., Murphy, S. M., de  
1458 Gouw, J., Warneke, C., and Jonsson, H. H.: Aerosol and gas re-distribution by shallow cumulus  
1459 clouds: An investigation using airborne measurements, *J Geophys Res-Atmos*, 117, n/a-n/a,  
1460 10.1029/2012jd018089, 2012.
- 1461 Wonaschütz, A., Hersey, S. P., Sorooshian, A., Craven, J. S., Metcalf, A. R., Flagan, R. C., and  
1462 Seinfeld, J. H.: Impact of a large wildfire on water-soluble organic aerosol in a major urban area:  
1463 the 2009 Station Fire in Los Angeles County, *Atmos Chem Phys*, 11, 8257-8270, 10.5194/acp-  
1464 11-8257-2011, 2011.
- 1465 Xian, P., Reid, J. S., Atwood, S. A., Johnson, R. S., Hyer, E. J., Westphal, D. L., and Sessions,  
1466 W.: Smoke aerosol transport patterns over the Maritime Continent, *Atmos Res*, 122, 469-485,  
1467 10.1016/j.atmosres.2012.05.006, 2013.
- 1468 Xu, J., Tian, Y., Cheng, C., Wang, C., Lin, Q., Li, M., Wang, X., and Shi, G.: Characteristics and  
1469 source apportionment of ambient single particles in Tianjin, China: The close association  
1470 between oxalic acid and biomass burning, *Atmos Res*, 237, 104843,  
1471 10.1016/j.atmosres.2020.104843, 2020.
- 1472 Xue, H., Khalizov, A. F., Wang, L., Zheng, J., and Zhang, R.: Effects of dicarboxylic acid  
1473 coating on the optical properties of soot, *Phys Chem Chem Phys*, 11, 7869-7875,  
1474 10.1039/b904129j, 2009.
- 1475 Yamasoe, M. A., Artaxo, P., Miguel, A. H., and Allen, A. G.: Chemical composition of aerosol  
1476 particles from direct emissions of vegetation fires in the Amazon Basin: water-soluble species  
1477 and trace elements, *Atmos Environ*, 34, 1641-1653, 10.1016/s1352-2310(99)00329-5, 2000.
- 1478 Yang, H., Yu, J. Z., Ho, S. S. H., Xu, J., Wu, W.-S., Wan, C. H., Wang, X., Wang, X., and  
1479 Wang, L.: The chemical composition of inorganic and carbonaceous materials in PM<sub>2.5</sub> in  
1480 Nanjing, China, *Atmos Environ*, 39, 3735-3749, 10.1016/j.atmosenv.2005.03.010, 2005.
- 1481 Yao, X., Fang, M., and Chan, C. K.: Size distributions and formation of dicarboxylic acids in  
1482 atmospheric particles, *Atmos Environ*, 36, 2099-2107, 10.1016/s1352-2310(02)00230-3, 2002.
- 1483 Yao, X., Lau, A. P. S., Fang, M., Chan, C. K., and Hu, M.: Size distributions and formation of  
1484 ionic species in atmospheric particulate pollutants in Beijing, China: 2—dicarboxylic acids,  
1485 *Atmos Environ*, 37, 3001-3007, 10.1016/s1352-2310(03)00256-5, 2003.
- 1486 Youn, J. S., Wang, Z., Wonaschutz, A., Arellano, A., Betterton, E. A., and Sorooshian, A.:  
1487 Evidence of aqueous secondary organic aerosol formation from biogenic emissions in the North  
1488 American Sonoran Desert, *Geophys Res Lett*, 40, 3468-3472, 10.1002/grl.50644, 2013.



- 1489 Yu, J. Z., Huang, X.-F., Xu, J., and Hu, M.: When Aerosol Sulfate Goes Up, So Does  
1490 Oxalate: Implication for the Formation Mechanisms of Oxalate, *Environ Sci Technol*, 39, 128-  
1491 133, 10.1021/es049559f, 2005.
- 1492 Yuan, H., Wang, Y., and Zhuang, G.: MSA in Beijing aerosol, *Chinese Sci Bull*, 49, 1020-1025,  
1493 10.1007/bf03184031, 2004.
- 1494 Zeng, G., Kelley, J., Kish, J. D., and Liu, Y.: Temperature-dependent deliquescent and  
1495 efflorescent properties of methanesulfonate sodium studied by ATR-FTIR spectroscopy, *J Phys*  
1496 *Chem A*, 118, 583-591, 10.1021/jp405896y, 2014.
- 1497 Ziemba, L. D., Griffin, R. J., Whitlow, S., and Talbot, R. W.: Characterization of water-soluble  
1498 organic aerosol in coastal New England: Implications of variations in size distribution, *Atmos*  
1499 *Environ*, 45, 7319-7329, 10.1016/j.atmosenv.2011.08.022, 2011.

1500



1501 **Table 1:** Seasonal concentrations ( $\text{ng m}^{-3}$ ) of organic acids and MSA for all (0.056 – 18  $\mu\text{m}$ ), submicrometer (0.056 – 1  $\mu\text{m}$ ), and  
 1502 supermicrometer (1 – 18  $\mu\text{m}$ ) sizes measured in Metro Manila from July 2018 to October 2019. n = number of sets.

Size/Species	All (n = 54)		SWM18 (n = 11)		Trans (n = 3)		NEM (n = 27)		SWM19 (n = 13)		
	Range	Mean (SD)	Range	Mean (SD)	Range	Mean (SD)	Range	Mean (SD)	Range	Mean (SD)	
All: 0.056 - 18 $\mu\text{m}$	Phthalate	0 - 67.02	8.68 (13.77)	1.97 - 67.02	16.75 (24.80)	17.36 - 45.30	26.94 (15.91)	0 - 14.72	4.79 (4.37)	0-25.03	5.72 (7.41)
	Adipate	0 - 43.83	7.60 (9.38)	0 - 20.18	9.08 (8.82)	0.24 - 19.56	8.47 (9.97)	0 - 13.00	4.22 (3.77)	0 - 43.83	13.18 (14.66)
	Succinate	0 - 116.28	9.53 (22.25)	0 - 116.28	21.61 (43.10)	0 - 14.31	7.57 (7.19)	0 - 62.83	7.14 (13.63)	0 - 20.14	4.73 (7.43)
	Maleate	0 - 119.19	9.52 (19.66)	2.56 - 58.39	18.68 (14.89)	0.19 - 8.45	3.81 (4.23)	0 - 14.42	1.65 (3.65)	2.30 - 119.19	19.44 (34.04)
	Oxalate	37.67 - 472.82	148.59 (94.26)	49.83 - 472.82	177.86 (139.41)	179.42 - 365.10	252.17 (99.15)	51.62 - 421.82	143.65 (75.76)	37.67 - 214.62	110.21 (62.06)
	MSA	0.10 - 23.33	5.40 (5.23)	2.77 - 23.33	10.01 (6.60)	0.16 - 16.14	5.55 (9.18)	0.10 - 7.45	3.08 (2.02)	0.84 - 17.52	6.30 (5.38)
0.056 - 1 $\mu\text{m}$	Phthalate	0 - 64.53	5.61 (12.90)	0.51 - 64.53	14.78 (24.24)	9.14 - 39.62	20.23 (16.85)	0 - 9.38	1.64 (2.47)	0 - 8.51	2.72 (3.11)
	Adipate	0 - 31.57	4.27 (5.84)	0 - 15.94	6.10 (6.25)	0 - 10.99	5.53 (5.50)	0 - 10.64	2.51 (3.15)	0 - 31.57	6.09 (8.80)
	Succinate	0 - 108.47	7.35 (19.58)	0 - 108.47	18.54 (38.92)	0 - 13.54	7.31 (6.84)	0 - 52.42	4.25 (10.36)	0 - 15.68	4.32 (6.61)
	Maleate	0 - 108.65	9.17 (18.41)	2.56 - 57.73	18.39 (14.92)	0.19 - 8.45	3.81 (4.23)	0 - 14.42	1.63 (3.64)	2.30 - 108.65	18.27 (31.26)
	Oxalate	16.21 - 318.49	93.30 (61.81)	29.96 - 256.72	108.26 (75.45)	96.84 - 250.78	165.57 (78.28)	26.11 - 318.49	90.60 (58.45)	16.21 - 151.79	69.58 (39.62)
	MSA	0 - 21.32	5.01 (4.93)	2.41 - 21.32	9.25 (6.15)	0.08 - 15.58	5.33 (8.88)	0 - 7.45	2.90 (2.09)	0.84 - 16.22	5.72 (5.09)
1 - 18 $\mu\text{m}$	Phthalate	0 - 16.52	3.07 (3.27)	0 - 4.07	1.98 (1.65)	5.43 - 9.03	6.71 (2.01)	0 - 9.42	3.15 (2.63)	0 - 16.52	3.00 (4.99)
	Adipate	0 - 26.00	3.34 (4.94)	0 - 7.87	2.98 (3.17)	0 - 8.56	2.93 (4.87)	0 - 8.07	1.71 (2.20)	0 - 26.00	7.10 (7.98)
	Succinate	0 - 21.18	2.18 (4.53)	0 - 16.02	3.06 (4.90)	0 - 0.77	0.26 (0.44)	0 - 21.18	2.89 (5.36)	0 - 5.33	0.41 (1.48)
	Maleate	0 - 10.54	0.35 (1.51)	0 - 2.30	0.29 (0.70)	0	0	0 - 0.45	0.02 (0.09)	0 - 10.54	1.17 (2.94)
	Oxalate	6.27 - 216.10	55.29 (38.52)	19.87 - 216.10	69.60 (67.47)	62.90 - 114.32	86.60 (25.95)	18.51 - 104.88	53.05 (22.89)	6.27 - 103.58	40.63 (28.89)
	MSA	0 - 2.00	0.40 (0.50)	0 - 2.00	0.75 (0.55)	0 - 0.56	0.21 (0.30)	0 - 1.58	0.18 (0.36)	0 - 1.93	0.58 (0.56)

1503



1504 **Table 2:** Contributions of the five positive matrix factorization (PMF) source factors to each  
1505 individual organic acid and MSA.

	<b>Combustion</b>	<b>Biomass Burning</b>	<b>Crustal</b>	<b>Sea Salt</b>	<b>Waste Processing</b>
<b>Phthalate</b>	27.4 %	49.5 %	13.3 %	9.9 %	0 %
<b>Adipate</b>	32.9 %	26.4 %	35.9 %	4.7 %	0 %
<b>Succinate</b>	0 %	90.3 %	9.7 %	0 %	0 %
<b>Maleate</b>	69.7 %	0 %	0.2 %	0 %	30.1 %
<b>Oxalate</b>	32.9 %	25.4 %	31.2 %	0 %	10.5 %
<b>MSA</b>	57.4 %	41.2 %	0.1 %	0 %	1.4 %

1506

1507

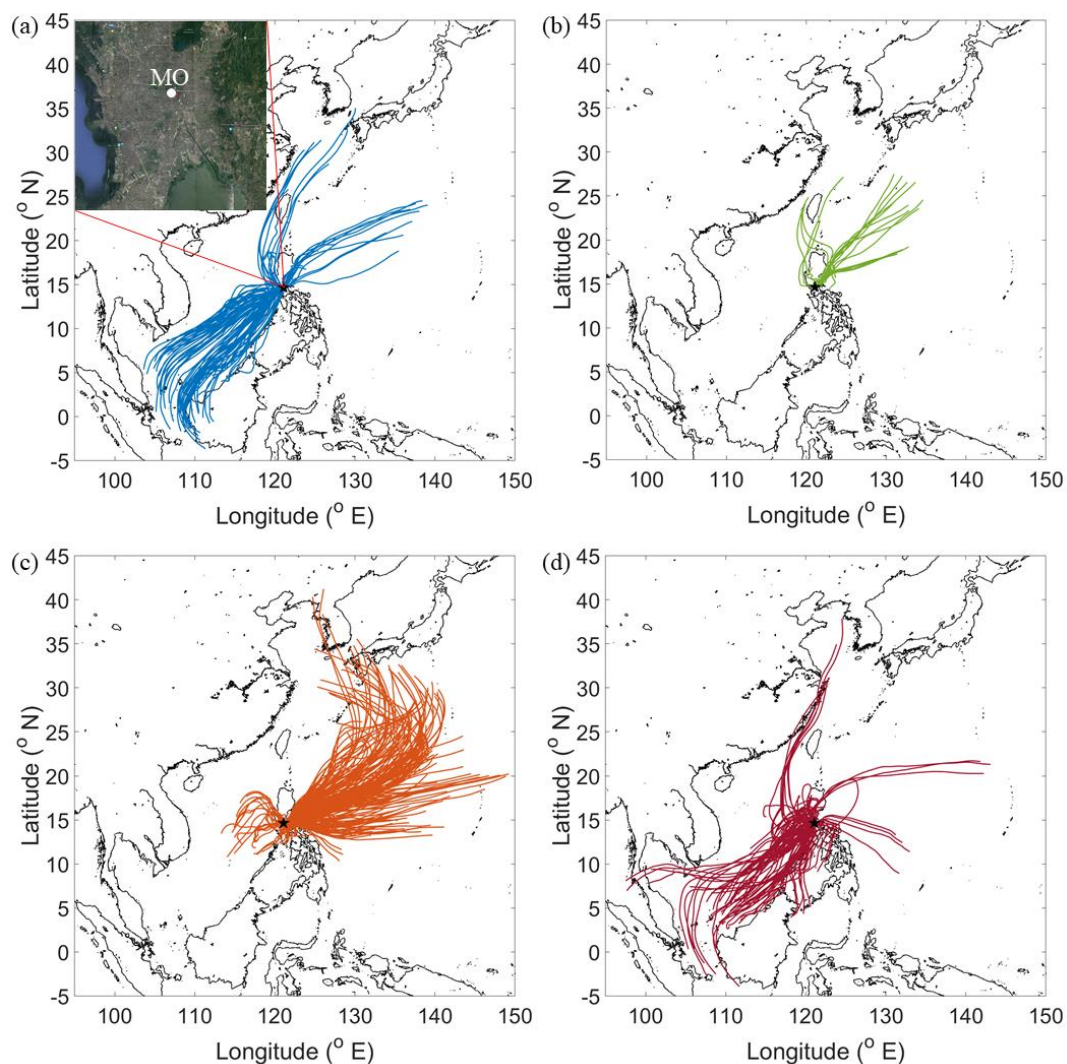


1508 **Table 3:** Pearson’s correlation matrices (r values) of water-soluble species for submicrometer  
 1509 (0.056 – 1.0 μm) and supermicrometer (1.0 – 18 μm) sizes. Blank boxes indicate p-values  
 1510 exceeding 0.05 and thus deemed to be statistically insignificant. Ad – adipate, Su – succinate,  
 1511 Ma – maleate, Ox – oxalate, Ph – phthalate. A similar correlation matrix for the full size range  
 1512 (0.056 – 18 μm) is in Table S6.

< 1 μm																			
Al	1.00																		
Ti		1.00																	
K	0.91		1.00																
Rb	0.44		0.48	1.00															
V		0.28		0.36	1.00														
Ni		0.47		0.40	0.89	1.00													
As							1.00												
Cd					0.64	0.68		1.00											
Pb	0.41		0.32	0.27	0.28	0.40		0.42	1.00										
Na										1.00									
Cl	0.90		0.99	0.39					0.30		1.00								
NO3	0.76		0.82	0.28							0.84	1.00							
SO4				0.42	0.48	0.40							1.00						
MSA				0.39									0.60	1.00					
Ad															1.00				
Su		0.31		0.67								0.45	0.67	0.33	1.00				
Ma														0.32		1.00			
Ox		0.35		0.70	0.47	0.53						0.72	0.47		0.69		1.00		
Ph		0.37		0.53								0.39	0.67	0.45	0.82		0.57	1.00	
	Al	Ti	K	Rb	V	Ni	As	Cd	Pb	Na	Cl	NO3	SO4	MSA	Ad	Su	Ma	Ox	Ph

> 1 μm																				
Al	1.00																			
Ti	0.56	1.00																		
K			1.00																	
Rb	0.62		0.48	1.00																
V		0.40		0.31	1.00															
Ni		0.30				1.00														
As		0.37			0.33		1.00													
Cd					0.66	0.41	0.34	1.00												
Pb	0.43	0.45		0.36	0.51	0.45		0.65	1.00											
Na	0.49	0.42								1.00										
Cl	0.45	0.48								0.90	1.00									
NO3	0.38			0.32	0.41					0.64	0.30	1.00								
SO4	0.39		0.81	0.64						0.37	0.29	0.36	1.00							
MSA										0.32				1.00						
Ad															1.00					
Su	0.39			0.28						0.30						1.00				
Ma															0.57		1.00			
Ox	0.59	0.29		0.48						0.45	0.59	0.35			0.45			1.00		
Ph		0.29									0.34				0.30				1.00	
	Al	Ti	K	Rb	V	Ni	As	Cd	Pb	Na	Cl	NO3	SO4	MSA	Ad	Su	Ma	Ox	Ph	

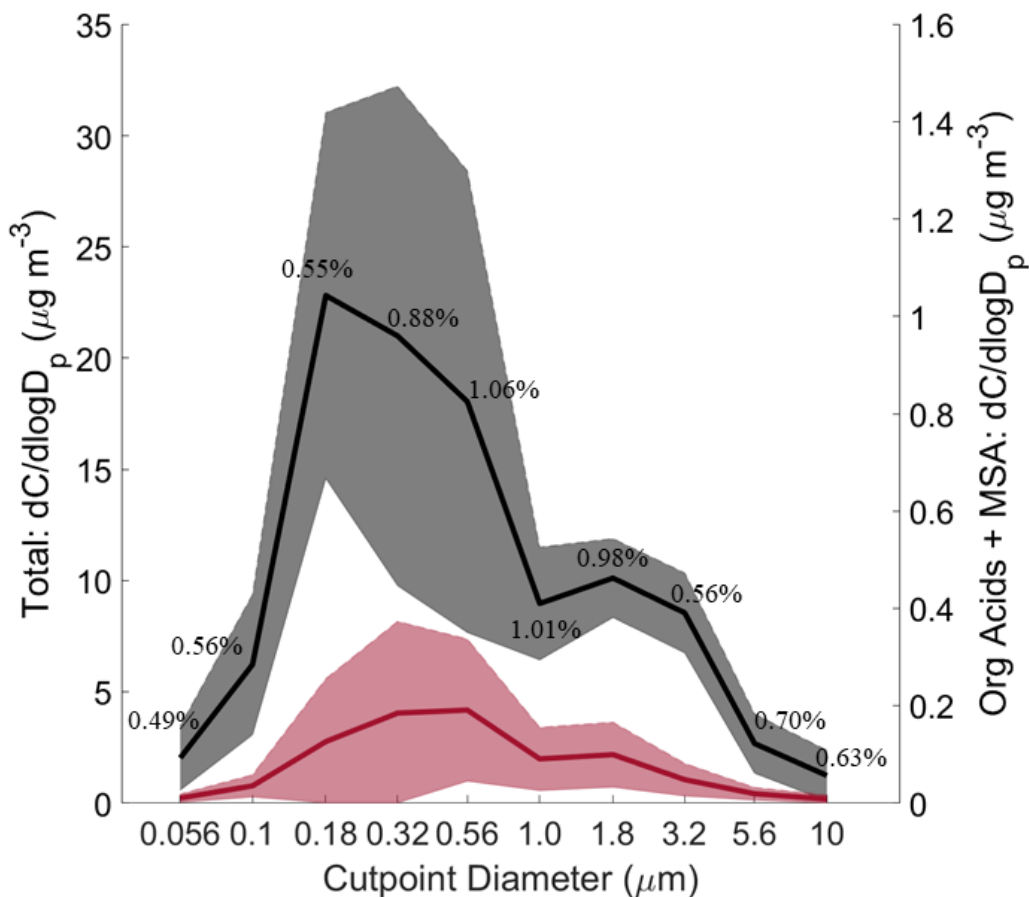
1513



1514

1515 **Figure 1:** HYSPLIT back-trajectories for four seasons: (a) 2018 southwest monsoon (SWM18),  
1516 (b) transitional period (Trans), (c) northeast monsoon (NEM), and (d) 2019 southwest monsoon  
1517 (SWM19). Results shown are based on 72-hour back-trajectories collected every 6 h during  
1518 sampling periods. The top left corner of panel (a) zooms in on Metro Manila with Manila  
1519 Observatory (MO) marked. The black star in each panel represents the sampling site. Map data:  
1520 © Google Earth, Maxar Technologies, CNES/Airbus, Data SIO, NOAA, U.S. Navy, NGA,  
1521 GEBCO.

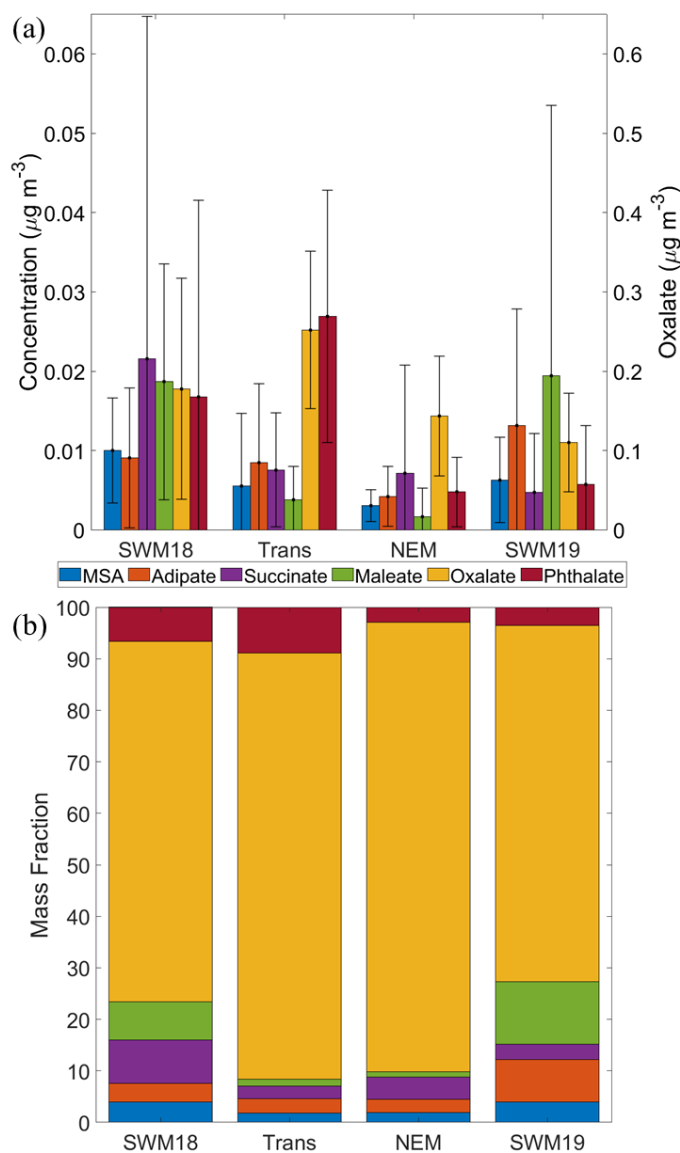
1522



1523

1524 **Figure 2:** Size-resolved comparison of total mass versus the sum of measured organic acids and  
1525 MSA. The black curve represents total mass and the red curve represents the summed organic  
1526 acids and MSA. Solid lines are the averages and shaded areas are one standard deviation. These  
1527 plots were made based on data from the 11 MOUDI chemical sets with accompanying  
1528 gravimetric measurements. The average percent contribution of the organic acids and MSA to  
1529 total mass is provided for each size bin. Refer to Fig. S1 for the seasonally-resolved version of  
1530 this figure.

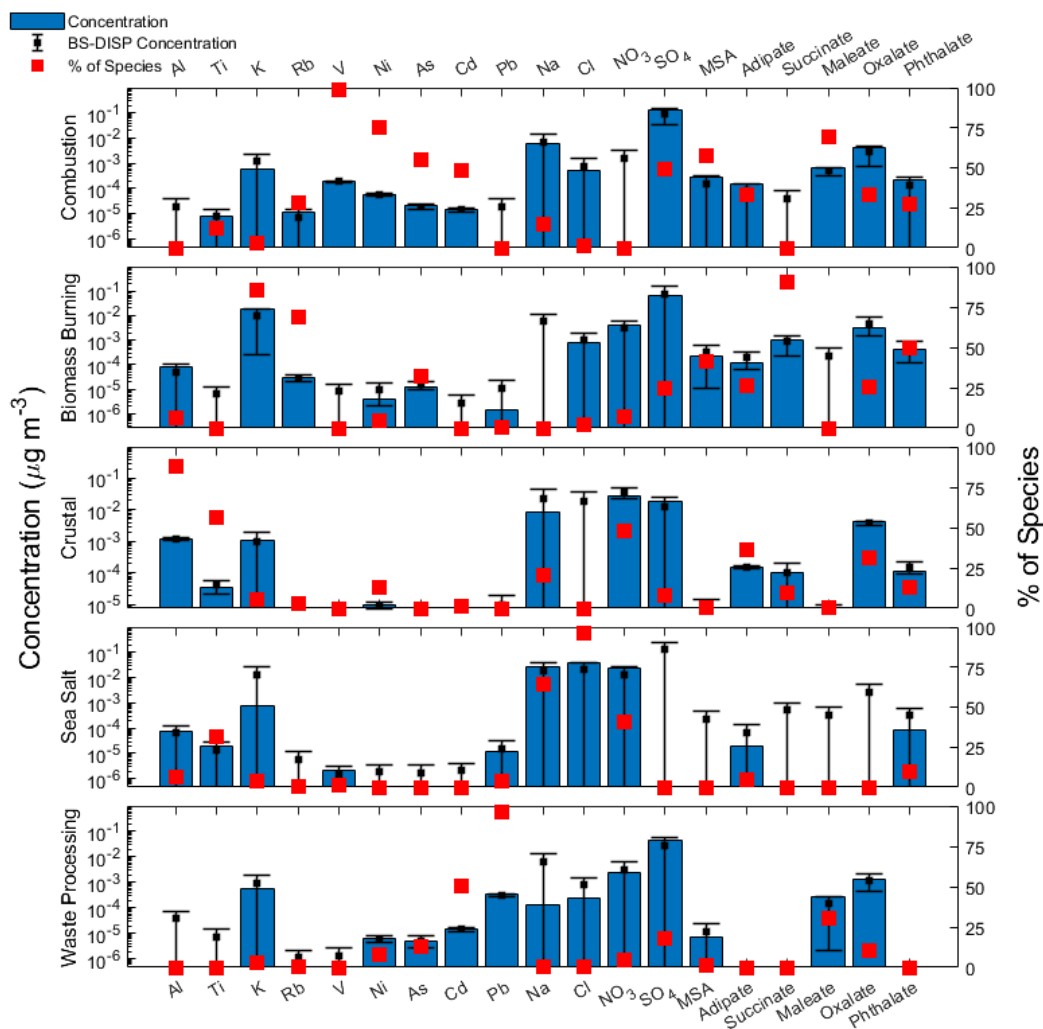
1531



1532

1533 **Figure 3:** (a) Average concentrations (0.056 – 18  $\mu\text{m}$ ) for (left y-axis) MSA, adipate, succinate,  
1534 maleate, and phthalate, in addition to (right y-axis) oxalate. Black bars represent one standard  
1535 deviation. (b) Percentage relative mass abundance of organic acids and MSA separated based on  
1536 season.

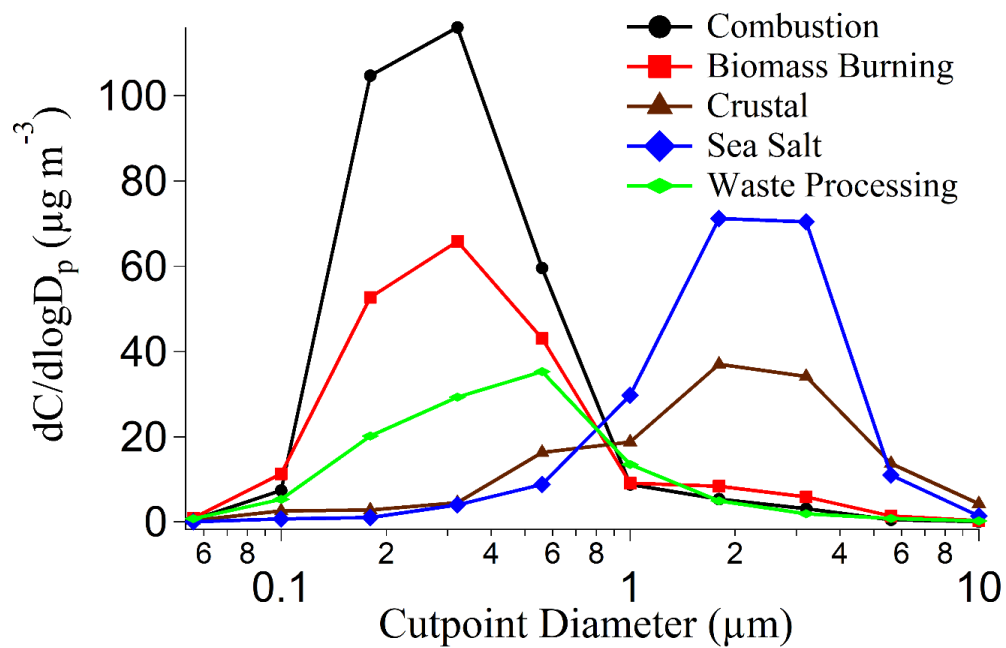
1537



1538

1539 **Figure 4:** Source factor profiles from positive matrix factorization (PMF) analysis. Blue bars  
 1540 represent the mass concentration contributed to the respective factor, red filled squares represent  
 1541 the percentage of total species associated with that source factor, and black squares with error  
 1542 bars represent the average, 5<sup>th</sup>, and 95<sup>th</sup> percentiles of bootstrapping with displacement (BS-  
 1543 DISP) values.

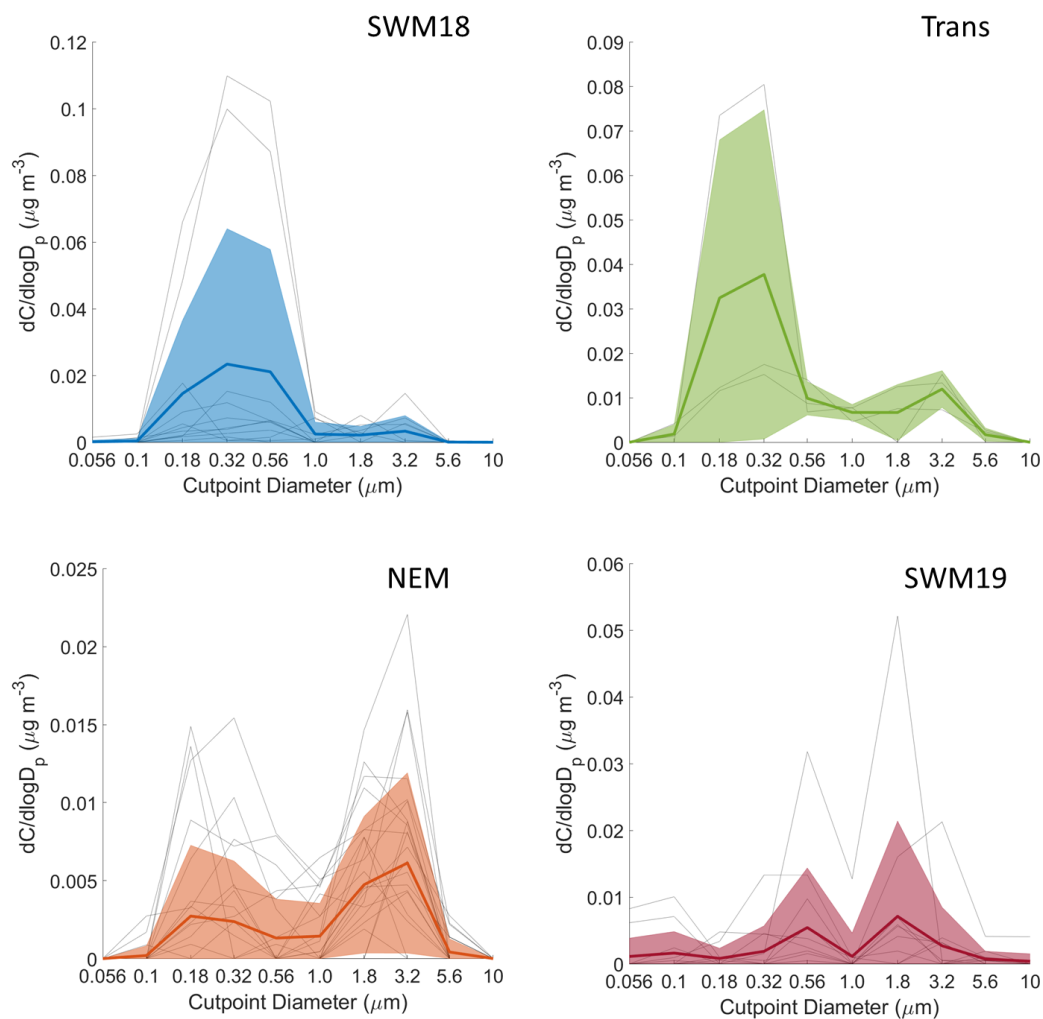
1544



1545

1546 **Figure 5:** Reconstructed mass size distributions of positive matrix factorization (PMF) factors.

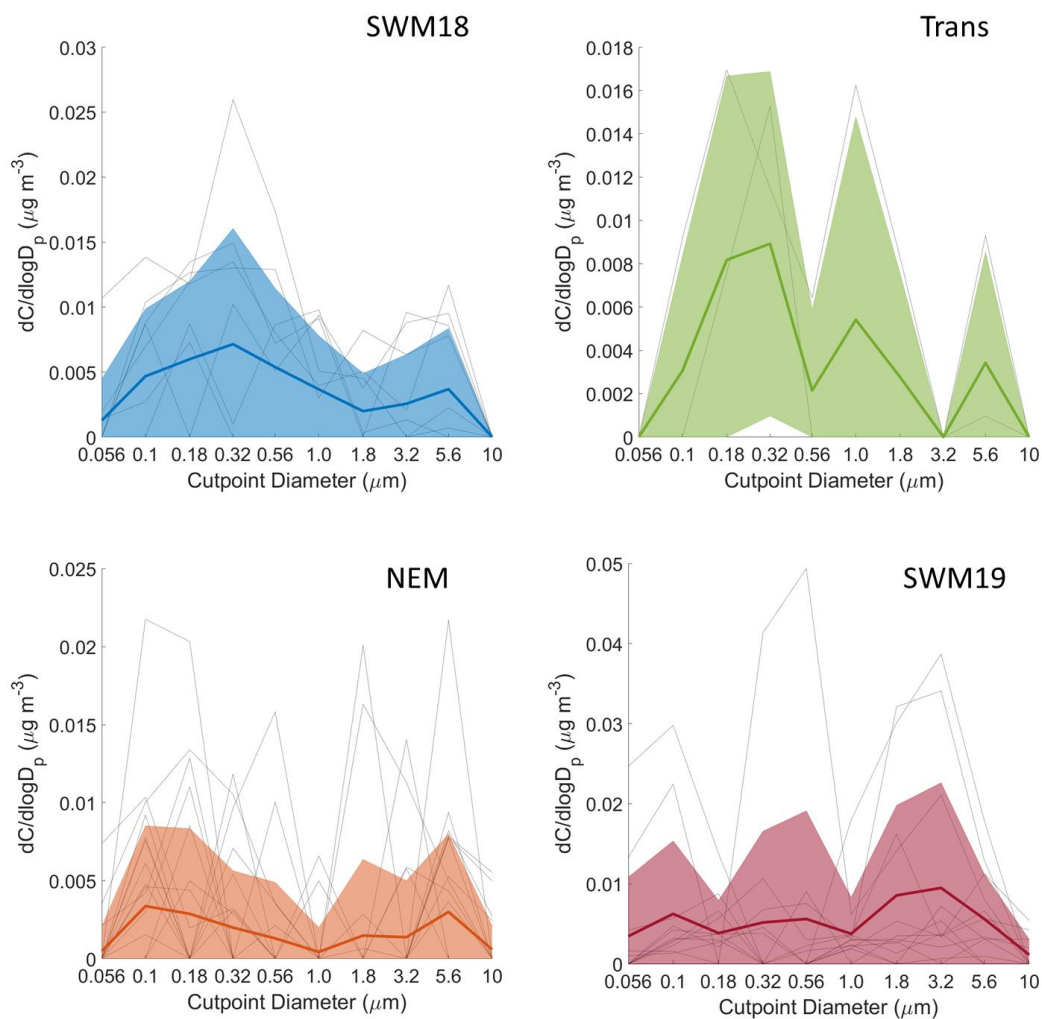
1547



1548

1549 **Figure 6:** Seasonal size distributions of phthalate. Gray lines represent individual sets, dark  
1550 colored lines are the average of all seasonal distributions, and transparent colored areas represent  
1551 one standard deviation. Note that the range of concentrations presented on the y-axis for each  
1552 season varies.

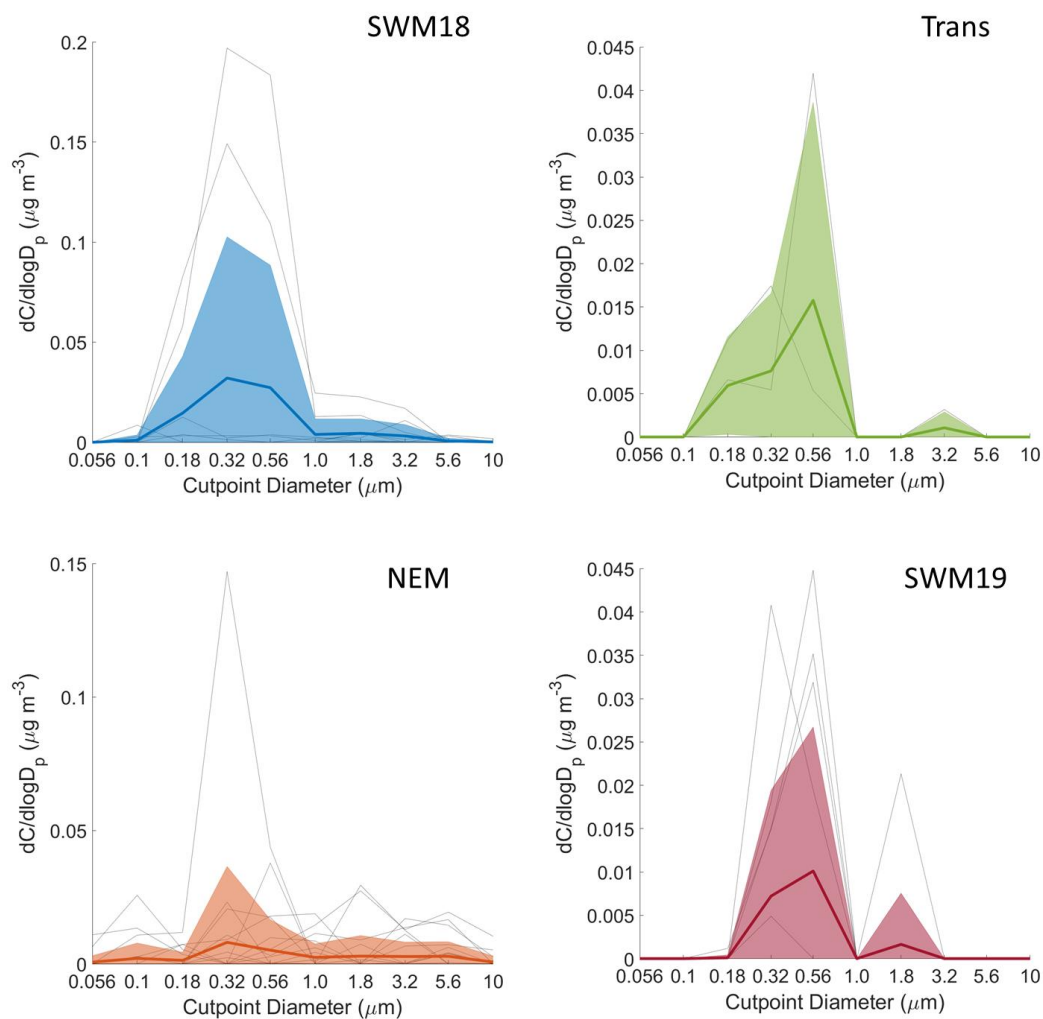
1553



1554

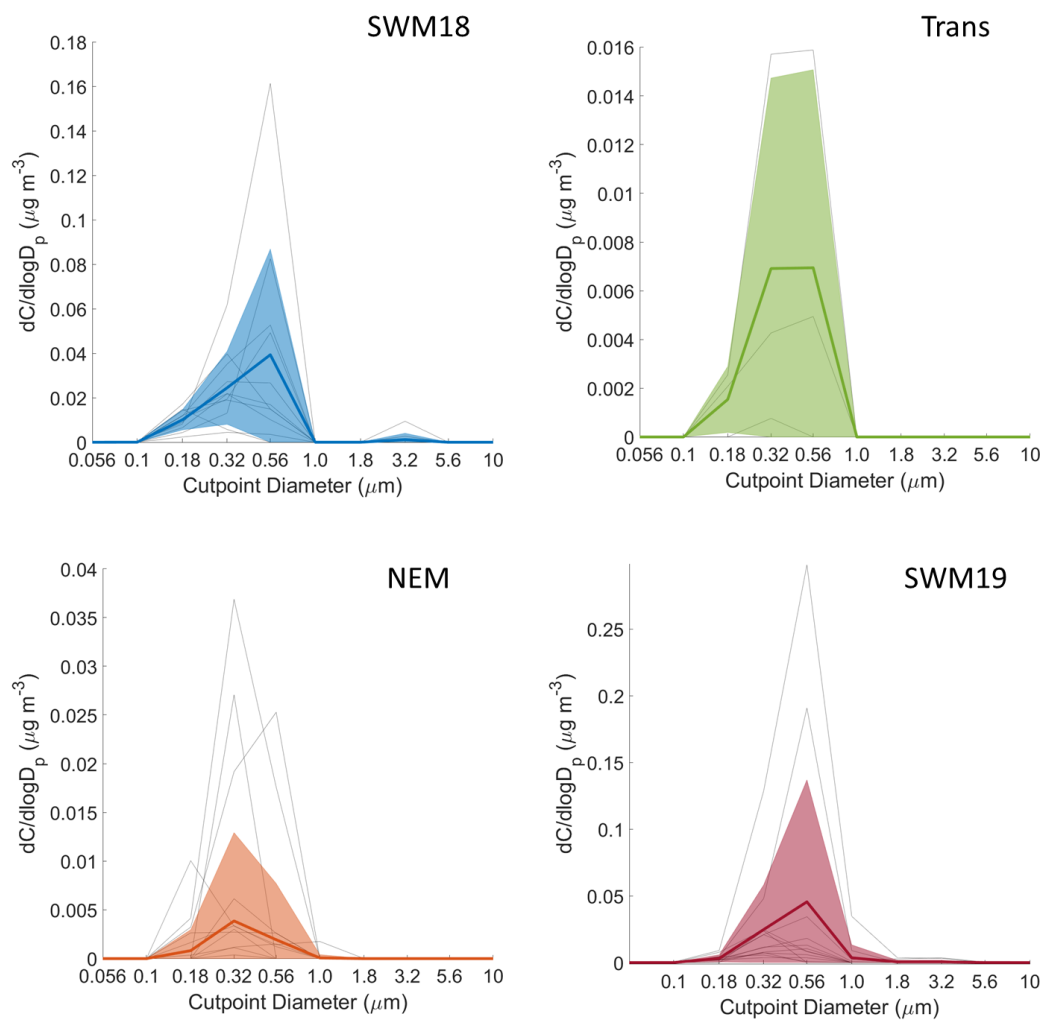
1555 **Figure 7:** Same as Fig. 6 but for adipate.

1556



1557

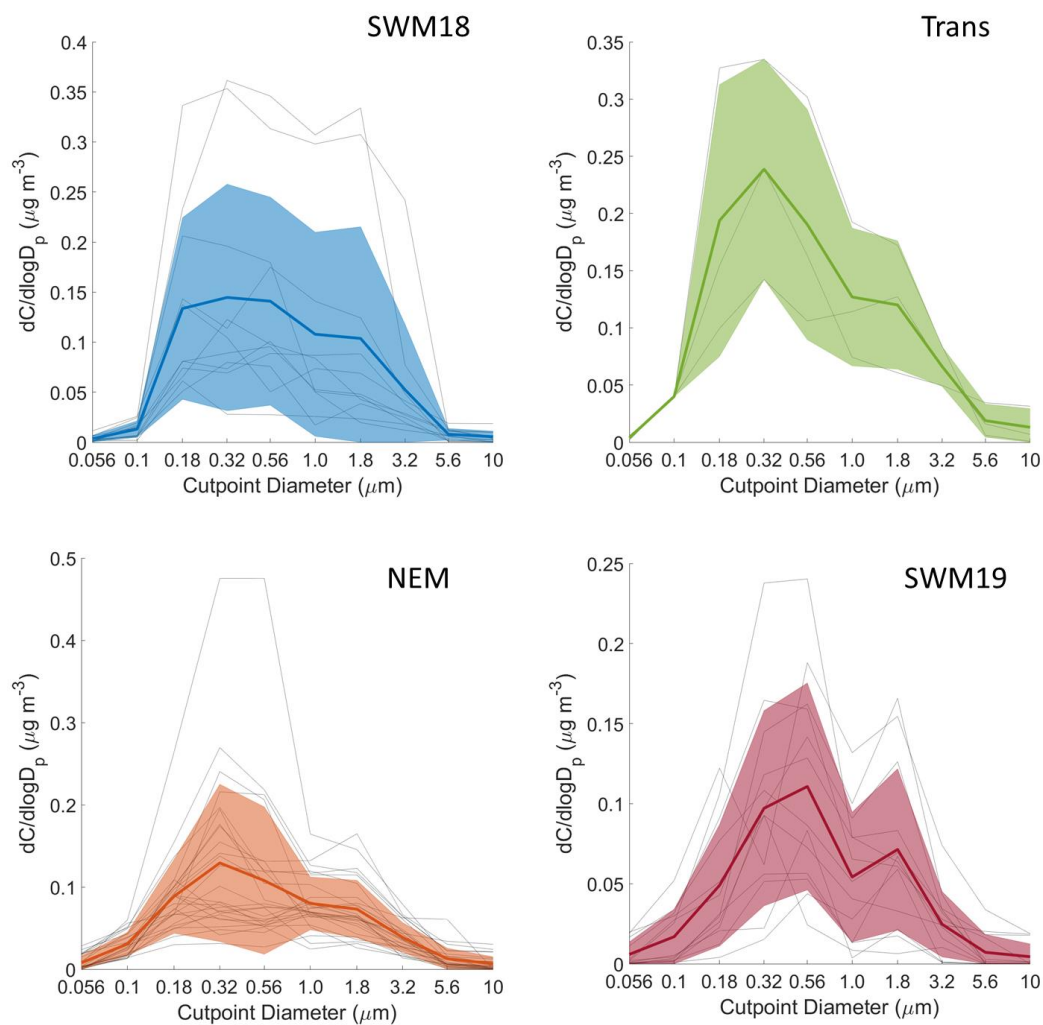
1558 **Figure 8:** Same as Fig. 6 but for succinate.



1559

1560 **Figure 9:** Same as Fig. 6 but for maleate.

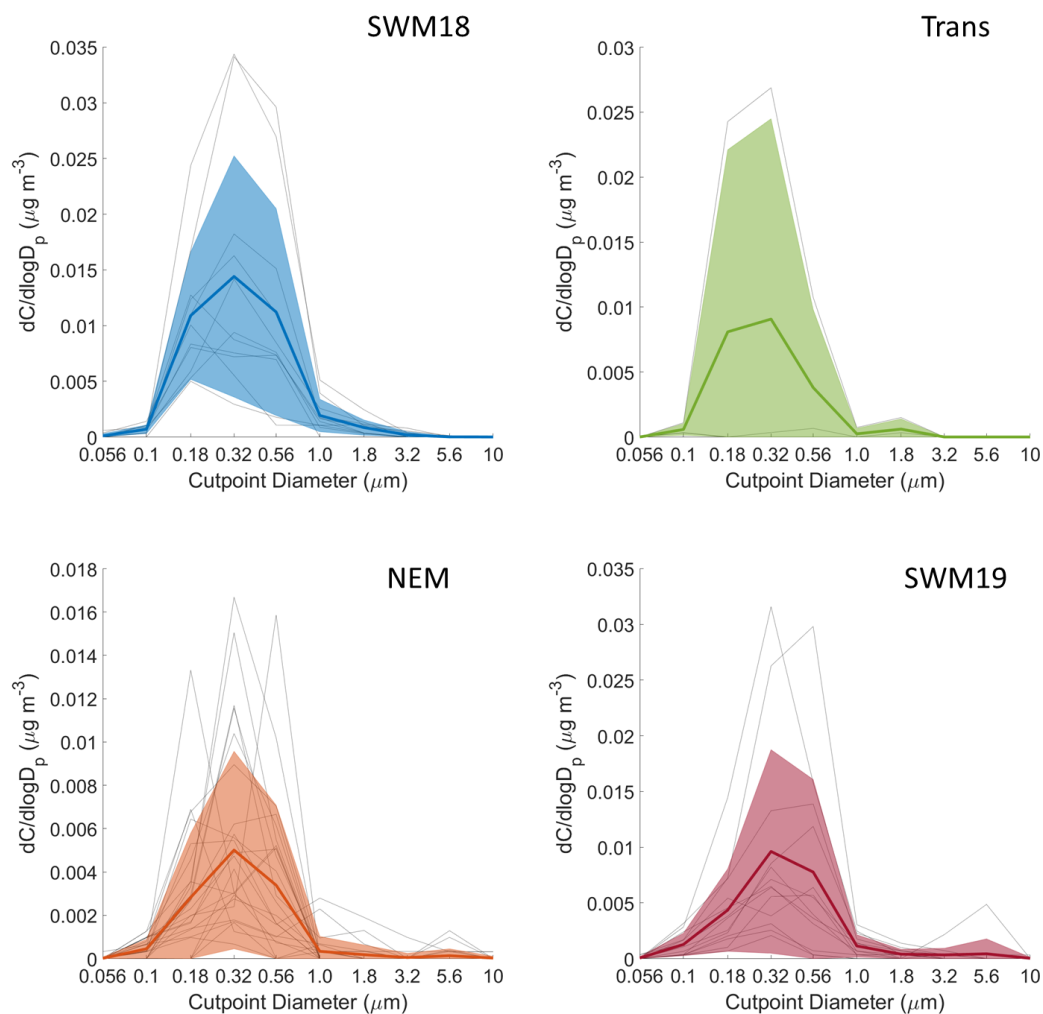
1561



1562

1563 **Figure 10:** Same as Fig. 6 but for oxalate.

1564

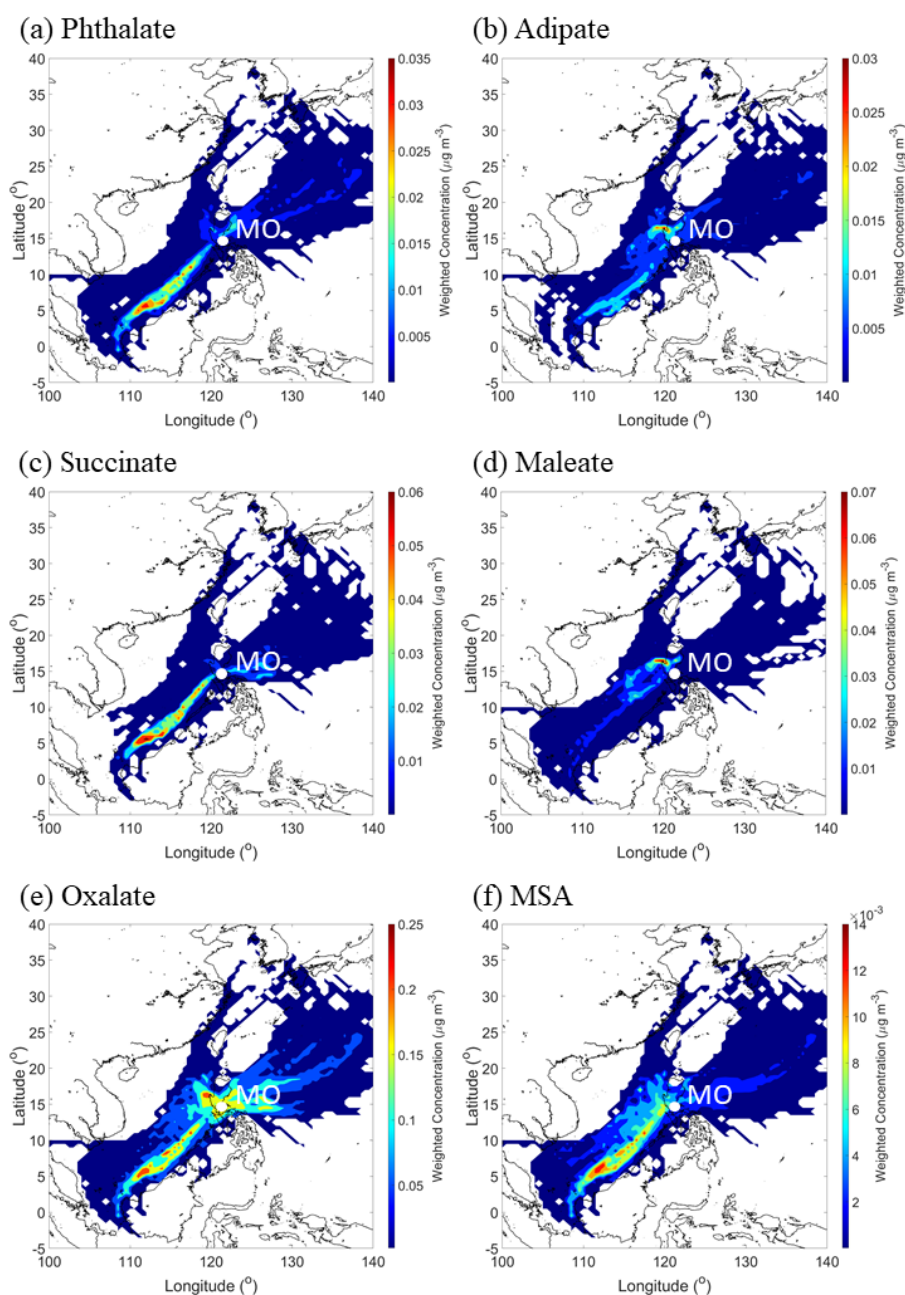


1565

1566 **Figure 11:** Same as Fig. 6 but for MSA.

1567

1568



1569

1570 **Figure 12:** WCWT maps of (a-e) individual organic acids and (f) MSA over the entire sampling  
1571 period. These results are based on all MOUDI sizes (0.056 – 18 µm). Maps showing the seasonal  
1572 results for each organic acid and MSA are shown in the Supplement (Figs. S3 – S8).